NTNU

Norwegian University of
Science and Technology

Design and analysis of a semi-submersible vertical axis wind turbine

Muhammad Abu Zafar Siddique

Preface

This thesis is submitted to the Norwegian University of Science and Technology (NTNU) for partial requirements to fulfill M.Sc. program.

This thesis is carried out the at the at the Department of Marine Technology under the supervision of Professor Zhen Gao at the department of Marine Technology, NTNU and the Co-supervisor Zhengshun Cheng. I am indebted to them. They helped me a lot and guide me to the proper direction. Also, I would like to thank Associate professor Erin Bachynski, Department of Marine Technology and PhD candidate Yuna Zhao who helped me to learn SIMA software. I would like to thank my colleague. They helped me a lot during my thesis.

The thesis was carried out from January 2017 to June 2017.

Abstract

Wind energy are deployed by two types of wind turbines. They are Horizontal Axis Wind Turbine (HAWT) and Vertical Axis Wind Turbine (VAWT), classified according to their axis of rotation. In recent years, offshore wind energy playing a vital role in the wind turbine industry due to high intensity of air, less turbulent and comparatively clean and easily employed in large area which is difficult to manage for onshore or near-shore. The advantages of HAWTs are now facing different challenge in the offshore field due to its cost effectiveness . For this reason, VAWTs have the potential to reduce the cost of producing per unit power. Hence, the emergence and growing interest for VAWTs for offshore application.

The availability of fully coupled simulation tools are extremely limited and more sophisticated tools are necessary to carry out the simulation in a fully coupled manner. In this thesis, we used SIMO-RIFLEX-AC for the fully coupled simulation developed by NTNU/MARINTEK. SIMO is capable to calculate the rigid body hydrodynamics forces and different moments on the floater which is designed to support the VAWT. RIFLEX is used to model the tower, blades, struts, mooring lines as flexible finite elements. To calculate the aerodynamic loads acting on the wind turbine we used Actuator Cylinder (AC) model. In addition, it accounts the effect of wind shear and turbulence, dynamic stall by using BL (Beddoes-Leishman) model and dynamic inflow. Then this code was coupled with SIMO-RIFLEX to carry out the integrated analysis.

To carry out the fully coupled simulation in time domain, a model was developed in HydroD and analyze the response in the frequency domain. The model was then modified in SIMO and used for coupled simulation. This model is used to study the various cases such as decay test, steady wind test and turbulent and irregular wave test. Also, we carried out a study on the second order mean drift force to check the response of the system. To calculate the second order effect, we use Newman approximation, otherwise to evaluate the second order transfer function is really time consuming. Then we compare our data with different types of vertical wind turbine such as OC4 semi-submersible and landbased wind turbine and carried out a detail study. We focus our study on motion response; performance of the wind turbine such as power, rotor speed, thrust, torque; mooring line tension and tower base bending moment. We also carried out power spectral analysis to see response in different frequency ranges. Considering three wind load cases such as one is below rated speed, one is the rated speed and the last one is above rated speed. The later study was carried out by using the WAFO which is used as a MATLAB routines.

One of the focus of the study is to optimize the original OC4 semi-submersible used to support the NREL 5MW wind turbine. The optimization was carried out in terms of reducing the weight and reducing the principal parameters of the platform which was carried out in the project. The optimization was satisfactory in terms of weight and its behavior because the modified OC4 semi-submersible preserve the main characteristics such as natural frequency and damping ratio.

In general, a fully coupled analysis was carried out to observe the dynamic characteristic of the wind turbine and applied the results to compare its characteristics with other floating and landbased

VAWTs. This will in turn helps us to reveal the advantages and disadvantages of using vertical axis wind turbine than horizontal axis wind turbine. Also, it will help to understand dynamic characteristics and behavior of different wind turbines.

Acknowledgement

First, I would like to express my immense gratitude to my supervisor Professor Zhen Gao to work under him. It's been almost one year since I started my work with him. Then I started to work for my thesis since January 2017. It's been five month since I worked with him for my thesis. During this period, we met once a week and discuss our work. He helped me and guide me like a true mentor. In this thesis, I always stumbled with some difficulty and professor was always there to help me. I was truly benefitted from his discussion, his insight on the topic.

Secondly, would like to thank my co-supervisor Zhengshun Cheng. I respect him for his patience on me during this time due to my silly question or silly mistake. He literally taught me the very foundation of the software that I used during my thesis. Sometimes I went to his room more than once in a single day. I spent hours to discuss and solve the problem. Whenever I stumbled, he helped me and show me the direction. He checked my code, correcting my error in the code. Often I sent him mail in the weekend and to my surprise he replied within two or three hours. I truly impressed not just as a knowledgeable person but his character and the patience I observed during this time.

Many other people helped me a lot in my thesis. Specially I would like to thank Associate professor Erin Bachynski for her support. Sometimes I ask her question through mail. Ph.D candidate Yuna Zhao who helped me how to use SIMA effectively. I would like to express my gratitude to my colleague and my friends who actively support my work.

I would like to give my special thanks to my parents who actively support me from my country Bangladesh. Also, my special thanks to my lovely wife Shanjida Hoque Sweety who helped me during this period immensely. I want to apologize not to give her enough time. Without them, I may never able to reach this far.

Finally, I want to thank Almighty Allah to bestow His immense mercy throughout my life.

Abbreviations

AC	*Actuator Cylinder*
BEM	*Blade Element Momentum theory*
CALHYPSO	*CALcul HYdrodynamique Pour les Structures Offshore*
CFD	*Computational Fluid Dynamics*
DLL	*Dynamic Link Library*
DMS	*Double Multi-Streamtube*
DOF	*Degrees of Freedom*
FHAWT	*Floating Horizontal Axis Wind Turbine*
FVAWT	*Floating Vertical Axis Wind Turbines*
GW	*Gigawatt*
HAWC2	*Horizontal Axis Wind turbine simulation Code 2nd generation*
HAWT	*Horizontal Axis Wind Turbine*
INFLOW	*INdustrialization setup of a FLoating Offshore Wind turbine*
ISO	*International Organization for Standardization*
JONSWAP	*Joint North Sea Wave Project*
LC	*Load Case*
MW	*Megawatt*
NACA	*National Advisory Committee for Aeronautics*
NREL	*National Renewable Energy laboratory*
OC4	*Offshore Code Comparison Collaboration Continuation*
OWENS	*Offshore Wind ENergy Simulation*
PI	*Proportional-Integral*
QTF	*Quadratic Transfer Function*
RAO	*Response Amplitude Operator*
RANS	*Reynolds-Averaged Navier Stroke*

TLP	*Tension Leg Platform*
USSR	*Union of Soviet Republics*
VAWT	*Vertical Axis Wind Turbine*
WADAM	*Wave Analysis by Diffraction and Morison Theory*
WAMIT	*Wave Analysis Massachusetts Institute of Technology*

List of symbol

α	*Angle of attack/Spectral parameter*
θ	*Angle*
γ	*Peaked parameter*
ε	*Phase angle*
ρ	*Density of water*
δ_{i3}	*Kronecker-Delta function for (i,3) component*
$\varphi(x, y, z, t)$	*Potential function*
ϕ_α^C	*Non-circulatory indicial function*
ϕ_α^l	*Circulatory indicial function*
η_i	*Platform motion*
ω_d	*Damping frequency*
ω_0	*Natural frequency*
ξ	*Damping ratio*
$\wedge$	*Logarithmic decrement*
ζ	*Wave elevation*
∇	*Vector operator*
A_{ij}	*Added mass matrix*
B_{ij}	*Damping matrix*
C_a	*Added mass coefficient*
C_d	*Drag coefficient*
C_{dz}	*Drag coefficient in the heave direction*
C_{ij}^{hydro}	*(i, j) component of from the linear hydrostatic restoring matrix*

List of symbol

C_L	*Lift coefficient*
C_N^v	*Normal force coefficient for vortex lift contribution*
C_p	*Power coefficient*
g	*Acceleration due to gravity*
H_s	*Significant wave height*
K_G	*Generator stiffness*
K_P	*Proportional gain*
K_I	*Integral gain*
K_D	*Derivative gain*
M_{ij}	*Mass Matrix*
n	*Normal vector*
p	*Pressure distribution*
Q_n	*Normal forces acting on actuator cylinder*
Q_t	*Tangential forces acting on actuator cylinder*
T_{ni}	*Time period*
T_p	*Peak time period*
T_{jk}^{ic}	*Quadratic transfer function*
V_0	*Volume displacement of water*
V_∞	*Free stream velocity*
(x_b, y_b, z_b)	*Center of buoyancy*
(x_g, y_g, z_g)	*Center of gravity*

List of figures

List of figures

List of tables

Contents

Contents

Contents

Chapter 1

Introduction

1.1　General background

The use of wind energy is not a new technology but draws its inspiration on the rediscovery of a long tradition of wind power technology. It's not possible to tell where and when the first wind harvesting procedure started but windmills are used to grinding grain and pumping water for at least several thousand years. In sailing ships the wind is an essential source of power for even longer. The spread of cheap coal and oil fuels and ease of energy distribution make people to forget this technology. They could only survive in the economic niches of little importance [1]. But in the of twentieth century people begin to realize how hazardous it can be for our environment and for us. It emits different types of greenhouse friendly gas such as CO_2, NO_x and SO_x. Fossil fuel might provide a cheaper source of energy but in turn it takes more than we can fathom. Also, the energy source is limited. So, they turn their attention into renewable energy source where people do not need to think the extinction of certain energy source. It helps our environment clean because no greenhouse gas emitted from it. Consequently, while energy production is based on the fossil fuel or splitting the uranium atom is meeting with increasing resistance or any other reason that might halt the progress, wind power is the inevitable consequence.

In modern times, the use of windmills to generate electricity can be traced to Charles Brush is the USA and the research was undertaken by Poul la Cour in Denmark. Another notable achievement was done Smith-Putnum. They developed a 1250 KW wind turbine with steel rotor 52 m in diameter. But in 1945, a blade spar failed catastrophically. Some author recorded that the 100 KW 30 m diameter Balaclava wind turbine in USSR in 1931 and the Andra Enfield 100 KW 24 m diameter pneumatic design constructed in the UK in the early 1950s. In Denmark, 200 KW 24m diameter Gedser machine was built in 1956. In 1963, Electricite de France tested a 1.1 MW 35 m diameter turbine in 1963 [2].

In the recent times, scientific community increases their investigation and develop new technique to harvest energy from wind. Worldwide there are now more than two hundred thousand wind

turbines operating, with a capacity of 432 GW at the end of 2015. Worldwide wind power generation capacity more than quadrupled between 2000 and 2006, doubling in every three years. The new installed capacity is mainly driven by the continuation of boom in Germany, China and USA which contributed to a capacity of 30.5 GW, nearly half of 63.01 GW installed in 2015. World wind capacity has expanded rapidly to 336 GW in June 2014 and energy production was around 4% of total worldwide electric power usage and growing rapidly. Europe accounted for 48% of the total wind power generation capacity in 2009. In 2010, Spain took the leading position in Europe and produces a total of 42,796 GWh. German held the top spot in Europe and their capacity was 27,215 MW as of 31 December 2010 [3]. The global wind power energy is increasing on a rapid scale by constructing megawatt scale wind turbine on land or at sea. Although the power industry is affected by the global economic crisis but GWEC predicts that the capacity of wind power will be 792.1 GW by the end of 2020.The figure shows the cumulative capacity of global wind power 1996-2015 and global annual installed capacity from 1997-2014.
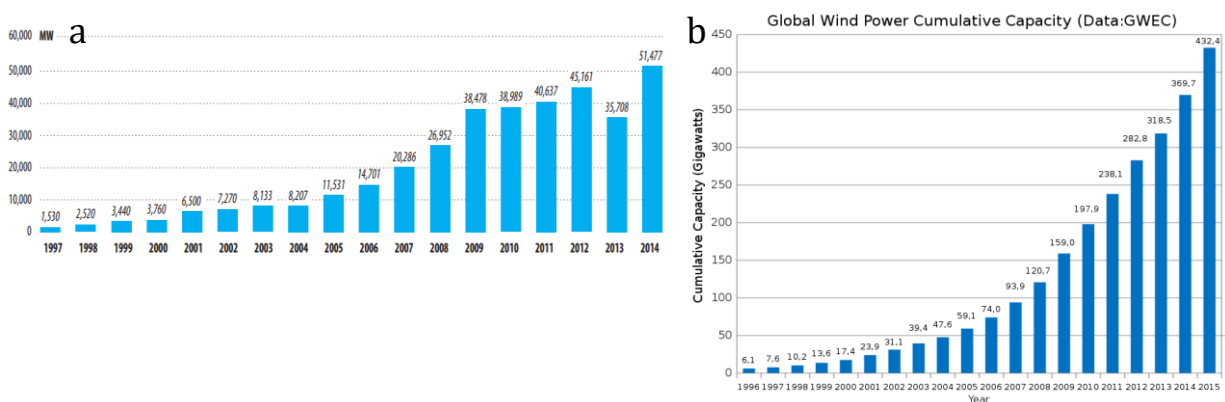
Figure 1.1: (a)Global annual installed capacity (1997-2014) (b) Global wind power cumulative capacity

Most of the wind farm are onshore based wind farm due to its cost effectiveness and maturity comparing to the offshore wind farm. Up to this date offshore wind energy covers only a small portion of the wind energy. By the end of 2015, it reaches 12.11 GW by the end of 2015 [4]. But the power production increases day by day and it's a major player in the wind sector.

In general, current offshore wind turbines are mounted on the fixed structures such as monopile, jacket based structure or gravity platform. As the water depth increases, the only option left is floating structure. In some countries, such as Norway, China, Japan and USA, there is an increasing trend to exploit deep water offshore wind energy as wind is stronger, less turbulent and more consistent than near-shore or onshore. Subsequently they employed different floater to support the wind turbine such as spar, barge, TLP, Hywind, DeepCwind and WindFloat and others.

There are basically two types of wind turbines. Horizontal axis wind turbine (HAWT) and the vertical axis wind turbine (VAWT). They are classified according to the orientation of the rotor axis. Currently, most commercial wind turbine farm uses horizontal axis wind turbine due to its economic advantages over vertical axis wind turbine. The main problem with HAWT compared to VAWT is the low efficiency and the fatigue problems within the bearings and blades. This

happen due to the large load variation on the VAWT. But as researcher focused on the offshore wind turbine, traditional HAWT facing a lot of challenges. The main challenge related to the cost effectiveness and the bending moment due to its higher center of mass. But VAWT is suitable is the offshore wind farm due to its lower center of gravity, reduced machinery complexity, independent of the wind direction, ability to take advantages of turbulent and gusty winds, some of them have a constant chord which is easy to manufacture and most importantly an excellent potential to reduce the cost of total installation.

The development of floating VAWT is in its early stage. The availability of the fully coupled simulation tool is limited and needs more advanced tool which integratedly analyze hydrodynamics, structural dynamics, aerodynamics and control system.

1.2   Vertical axis wind turbine

There are two variants in the wind turbine. One is horizontal and the other one is vertical. For VAWT the main rotor shaft is set transverse to the wind and main components such as generator, shafts are located at the base. The arrangement facilitates the maintenance and repair due to the generator and gearbox are located close to the ground. They are categorized as drag driven type or lift driven type. The Savonius are usually drag driven type while the Darrieus and straight bladed VAWT are considered lift driven type. Other VAWT such as oval trajectory Darrieus turbine, Darrieus-Masgrowe rotor, crossflex turbine, combined Savonius and Darrieus rotor, Zephyr turbine etc [5].

Horizontal axis wind turbines are more efficient than vertical axis wind turbine. The cost is low compared to the later one. For this reason, they are dominating in the market and used for commercial purpose in large scale. Compared to HAWTs, the most critical thing that limits the use of VAWT were the low efficiency and fatigue problem. But the efficiency can be improved by optimizing the turbine distribution. But the fatigue problem is difficult to maintain. It happens when there is a large variation of the load acting on different components of the VAWT. It might be worthy to mention here that by using composite material or increasing the blade number helps us to reduce the fatigue problem. The main advantages of VAWT over HAWT is described below:

- They are omni-directional. So, we don't need to employ different machinery such as yaw control to track down the flow of air.
- Ability to take advantage of turbulent and gusty wind. This might accelerate the fatigue problem in HAWT.
- Easy to maintain as gearbox and generator are at the ground level. Also, gearbox of a VAWT takes less fatigue than HAWT.
- Blades of VAWT are easy to manufacture. For example, Darrieus VAWT uses constant chord length which is easy to manufacture.
- Need less area for VAWT wind farm than HAWT farm.
- Excellent potential to upscale.

1.3   Floating VAWT

In offshore wind farm, VAWT has several advantages over HAWT as we mentioned earlier. Researcher are developing different kinds of floater to support VAWT. Different concepts are developed in the last decades and still different concepts are emerging. Some of them are DeepWind, Spinfloat, INFLOW, Gwind and floating tilted axis wind turbine [5].

The DeepWind project consists of a vertical axis wind turbine mounted on a floating spar buoy. The vertical axis turbine based on the concept Darrieus rotor 5 MW capacity and includes a direct drive generator with its electronic control system. The concept was evaluated in Hywind test site. The feasibility of upscaling from 5MW-20MW [6].

The Gwind concept was developed by Norwegian Gwind research project. A gyro stabilizer stabilizes the floating VAWT. A prototype named Spinwind 1, to explore the dynamic characteristic of the concept.

The industrialization setup of Floating Offshore Wind Turbine (INFLOW) project participates in the development of an innovative solution for the offshore wind market. A 2 MW optimized system with two contra-rotating wind turbines with two straight blades. The floating support of the first 2 MW offshore prototype to be tested in the INFLOW project is still a tri-floater system. This project will rely on the results of the onshore wind turbine prototype of the VERTIWIND project [7]. Some figures are attached below for different FVAWT.
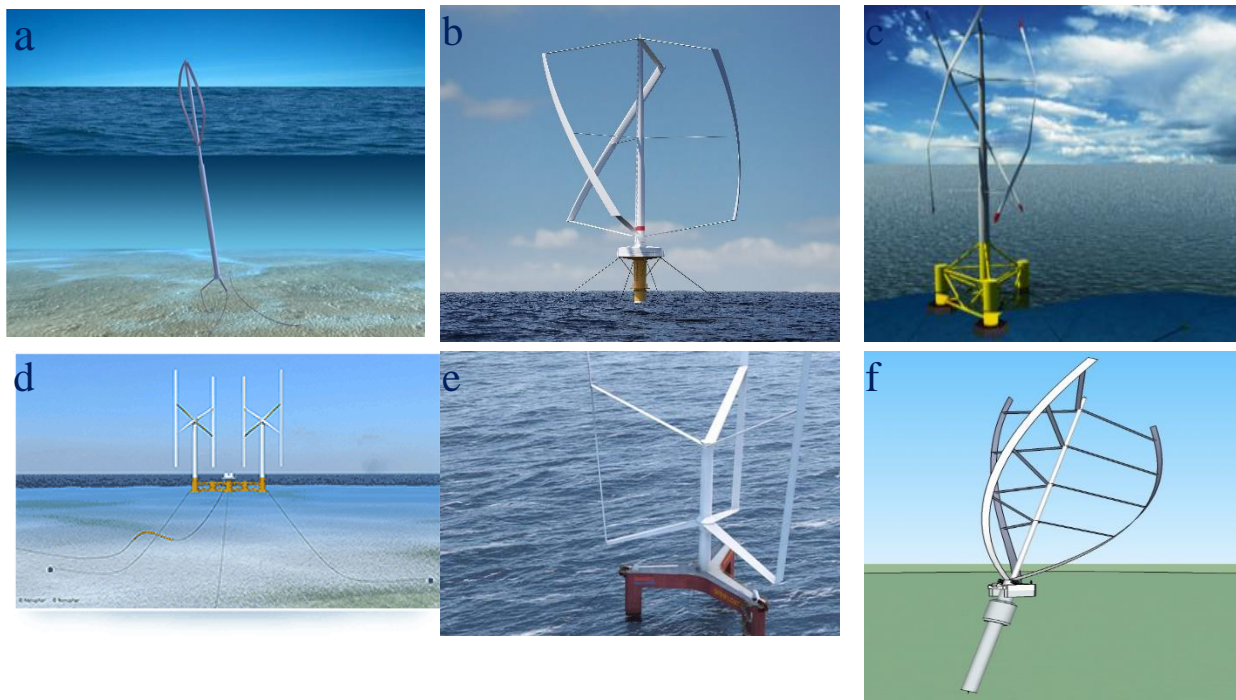
Figure 1.2: (a)DeepWind concept (b)Gwind concept (c)VertiWind concept (d) INFLOW concept (e) Spinfloat concept (f) Tilted axis concept

1.4 State of art in VAWT and HAWT modelling

We mentioned earlier, HAWTs are the main focus of the wind energy industry, the technology is more mature than VAWTs. VAWTs lost its ground due to its low efficiency and fatigue issues. The maximum efficiency a turbine can achieve is 59.3% which is known as Betz limit. HAWTs are more efficient than VAWTs. The efficiency for HAWTs up to 50% while for VAWTs the efficiency is approximately 40% [8].

Major driving point to design the floating turbine is the scalability. HAWT have this limitation due to the gravitational fatigue as the blades undergo tension-compression cycle. As for VAWT we do not have such problem. HAWTs have gravitational fatigue issues, VAWTs produces cyclically varying torque that can have adverse effect on transmission and control systems. Due to the advancement of material technology we can easily solve this problem by using composite materials [9].

As we discussed earlier, machinery in VAWTs can be handled more effectively than HAWTs. In VAWTs the machinery placed in the bottom of the tower while for HAWTs the nacelle is placed at the top of the tower. This is one of the reason the cost for maintenance for HAWTs is higher than VAWTs.

1.4.1 Aerodynamic modelling

The aerodynamic model used for VAWTs are Blade Element Momentum theory (BEM), Cascade model, Vortex mode, Actuator Cylinder model (AC). Reynolds-averaged Navier Stokes (RANS) model and Computational Fluid Dynamics (CFD) used very complicated and computationally intensive method.

BEM is used to calculate the load acting on the wind turbines blade. This theory combines both blade element theory and momentum theory. The first momentum model for VAWTs was developed by Templin, where a single streamtube passing through an actuator disk to represent VAWT. Wilson and Lissaman developed the multi streamtube model. The DMS model is one of the most used model to calculate the aerodynamic loads on the wind turbine. [8].

Cascade model was first developed by Hirsch and Mandal to apply the cascade principal to analyze the VAWTs. To improve the analytical capability of this model, Mandal and Burton use dynamic stall and streamline curvature in the model. This model demands more computational time than momentum model but it gives more accurate results for both low and high solidity rotors [10].

Vortex model assumes potential flow. The velocity field obtain by calculating the influence of vorticity in the wakes of the blades. Larsen [11] proposed a 2D vortex model and advanced by Fanucci and Walter [12], Holmes [13] and Wilson [14] Their model assumes high tip speed ratio, lightly loaded rotor, small angle of attack to ignore stall. These assumption limits the applicability of the model. The first versatile 3D vortex model was proposed by Strickland et al [15]. Later

Strickland employed dynamic effects, dynamic stall model, pitching circulation and added mass in the model. To accelerate the model Cardona [16] proposed a flow curvature as well as modifying the dynamic stall model.

The AC model is a quasi-static Eulerian model. The AC model was first developed from the PhD study carried by Madsen et al. [17]. The basic idea is to use the known AD flow model from HAWT and to develop a general approach of an actuator surface coinciding with the swept area of the actual turbine [17]. For a straight bladed VAWT the swept surface area is cylindrical. To reduce the complexity of the model this model is a 2D representation of the general model.

1.4.2   Couple analysis tool

To this date, several coupled analysis tools were developed for FVAWT. Some of them are CARDAAX was developed by Paraschivoiu [18] who implemented the DMS model to carry out the VAWT analysis [8].

Strickland [19] developed two and three-dimensional vortex model VDART2 and VDART3 in 1970s as a part of Sandia National Laboratories effort to develop an analysis tool for VAWT. While Dixon [20] developed three-dimensional unsteady panel model in Delft University of Technology and the name of the code is UMPM (Unsteady free wake Multi-Body Panel Method) [8].

SIMO-RIFLEX-AC and SIMO-RIFLEX-DMS was developed by NTNU. The former one was developed by Cheng et al. [21] in his thesis while the later one was developed by Wang et al. to perform the fully coupled analysis for floating VAWTs. In this study, we use actuator cylinder model to calculate the aerodynamic loads on the wind turbine. The code was based on the work of Madsen et al. [17] while doing his Ph.D. thesis. The code was then coupled with SIMO and RIFLEX. It integrates the aerodynamic loads, hydrodynamic loads, structural dynamics, control system and mooring dynamics in a fully coupled way. The hydrodynamic loads are calculated by the SIMO where it considers the platform as rigid body. The hydrodynamic loads are calculated based on potential flow theory and Morison's model for slender body. The tower, shaft, mooring lines which are designed as flexible finite elements, are solved by using non-linear FEM solver. While calculating the aerodynamic loads on the wind turbine based on AC method, it also considers the shear effect of wind and Beddoes-Leishman dynamic stall model. A generator torque controller was also implemented to regulate the rotor rotational speed based on the PI algorithm [5].

HAWC2 also apply the AC method to calculate the aerodynamic loads on VAWTs. HAWC2 was originally developed for the couple analysis of HAWTs, later developed for VAWTs [22]. This software was developed DTU. To calculate the hydrodynamic loads on the platform it uses Morison equation and coupling with WAMIT [5].

Beside that some available tools used to analyze the VAWTs are OWENS (Offshore Wind Energy Simulation), developed by Sandia National Laboratories, CALHYPSO (Calcul Hydrodynamique

Poer les Structures Offshore), FloVAWT (Floating Vertical Axis Wind Turbine) developed by Cranfield University [5].

1.5   Aim and scope of the study

The purpose of this thesis is to design a OC4 semi-submersible offshore platform that will support a 5 MW vertical axis wind turbine. For this reason, a coupled analysis was developed in SIMO-RIFLEX-AC to observe the global response of the total system. The central focus of this thesis to observe the response in different wind and wave conditions. Also, we need to carefully select the principal parameter of the platform that will preserve the total stability of the system. Then the optimized system which is developed in this study need to be compared with the old OC4 semi-submersible. The basic task that will address in this study are the following:

- Based on the design of the semi-submersible from the project work, establish a time domain model in SIMO-RIFLEX-AC using the wind turbine model from the old OC4 concept. Care should be given to the adjustment of the mass and restoring matrix when the tower and the blades are modelled explicitly as RIFLEX beams. This topic will be address in chapter two and three.
- Perform decay tests to identify the natural periods and damping coefficients for the rigid-body motion modes. This topic will be discussed in chapter two.
- Perform time-domain simulations for the turbulent wind and irregular wave cases and compare the statistics and the spectra for the dynamic responses of the new semi-submersible wind turbine and the old OC4 wind turbine. This topic will be addressed in chapter three.
- Two analyze the second order drift effect on the system and then compare the difference in the first order prediction. This topic will be discussed on chapter four.

Chapter 2

Design and stability of Floating semi-submersible

2.1 Platform design

The design of a floating VAWT is pushed by two basic parameters:

- Structural integrity of the body.
- Static and dynamic stability of the body.

The total body comprised of two basic structure. The first one is OC4 semi-submersible and the second one is wind turbine. To float the wind turbine in this study, we designed a OC4 semi-submersible. Within the framework of OC4 (Offshore Code Comparison Collaboration, Continuation) projects, hydrodynamic calculation and code to code comparison were performed for NREL 5 MW wind turbine on top of the DeepCwind semi-submersible platform [23].

The DeepCwind semi-submersible is designed for 200 m depth, consists of one main column (MC) and three offset column (OC). On top of the main column, the 5MW wind turbine rested. Each offset column is divided into two parts. One upper column (UC) and the other one is known as base column (BC). The base column has larger diameter than the upper column. It also represents a heave plate which acted as suppression device. The center of the offset column arranged on top of an equilateral triangle whose edge length is 52 m. Offset column and main column are connected by braces and pontoons. Cross braces (CB) are connected to the bottom of the main column and pontoon are used to connect the offset and main column. Pontoons are divided into delta and Y pontoons. They are named due to their arrangement as seen from the figure. The upper and lower Y pontoon (YU and YL) are connected to main and offset column while the upper and lower delta are interconnected to the offset column (DU and DL). Before discussing on the stability, it's necessary to introduce the method of developing panel model in HydroD and the model.

To analyze the stability of the platform we first need to build a panel model for HydroD. The first task is to develop a FEM model in GeniE. As it involves a lot of iteration, in the first step, we create a parametric model in GeniE and by changing the parameter we can easily build a new platform. The principal step is listed below:

- Panel model (T1.FEM) which have distinctive wetted surface define by GeniE and import in HydroD to calculate hydrostatic pressure and measure the buoyancy force. A panel model for a DeepCwind is shown in the following figure.

- Mass model (T2.FEM) contains all the mass matrix of the platform. A well-defined structural model is out of scope for this project. So, we use user defined option and input this value manually.
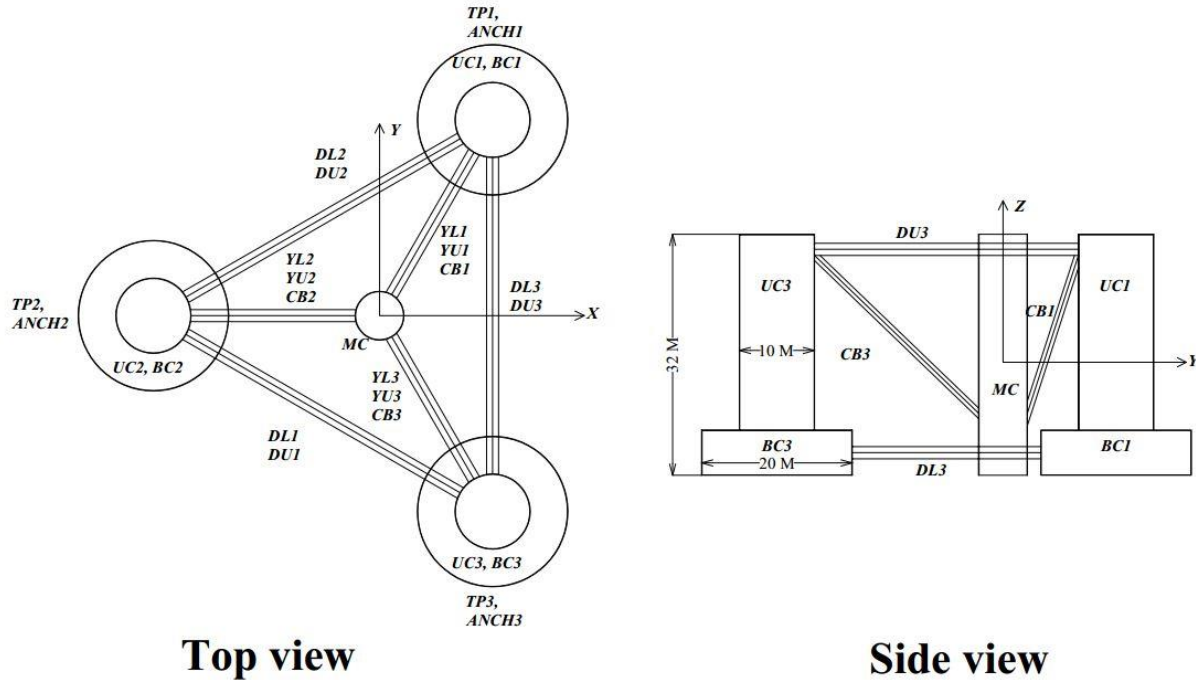
Figure 2.1: Layout of optimized OC4 semi-submersible

Table 2.1: Main specification of OC4 semi-submersible

Element	Diameter [m]	Thickness [m]	Length [m]	Drag coefficient
Main column	6.5	0.06	32	0.56
Upper column	10	0.06	26	0.61
Base column	20	0.06	6	0.68
Y- upper	1.6	0.0175	25.02	0.63
Y- lower	1.6	0.0175	20.02	0.63
Delta upper	1.6	0.0175	42	0.63
Delta lower	1.6	0.0175	32	0.63
Cross braces	1.6	0.0175	33	0.63

Density of the material	$7850\ kgm^{-3}$
Density of the fluid	$1025\ kgm^{-3}$
Total platform mass	$9857.6\ kg$
Center of gravity	(0 0 -11.9045)
Draft of the platform	20 m

The floating platform is moored with three catenary lines. Each line is $120^{°}$ apart from each other. They are used to secure the platform and restraint the movement. Lines are symmetrical about x axis. Fairleads are located at the top of the base column, at a depth 14 m below the SWL and connected to the anchor. The anchors are rested on the seabed, 200 m below the SWL. The following table summarizes all the necessary detail of the mooring lines. Also, the stability results for the new OC4 semi-submersible will be discussed at end of the this chapter.

Table 2.2: Specification of mooring line

Number of mooring lines	3
Angle between adjacent lines	$120^{°}$
Depth of anchor below SWL	200 m
Depth of fairleads below SWL	14 m
Radius of fairlead from the platform centerline	40.02 m
Radius of anchor from the platform centerline	835.5 m
Mooring line diameter	0.0766 m
Per unit mass density	113.35 kg/m
Hydrodynamic drag coefficient	1.1
Hydrodynamic added mass coefficient	1.0
Structural damping of mooring lines	2.0%

Table 2.3: Principal parameter of straight bladed wind turbine

Rated power [MW]	5.30
Blade number [-]	3
Rotor radius [m]	39
Rotor height [m]	80
Chord length [m]	2.7
Aerofoil section	NACA 0018
Tower top height [m]	79.78
Cut in, rated and cut out wind speed [m/s]	5.0, 14.0, 25.0
Rated rotational speed [rad/s]	1.08
Total mass, including rotor, shaft and tower [ton]	315.3
Center of mass for rotor [m]	(0, 0, 48.14)

2.2   Old OC4 Platform

One of the main objective of this study is to optimize the characteristic of the OC4 semi-submersible and compare the data to the old one. In this study, the parent OC4 semi-submersible, which was our base design and which was designed to support a three-bladed floating VAWT. For the straight-bladed rotors, the structural properties of the blades, struts, tower and shaft were determined based on the Deepwind rotor, 5MW Darrieus rotor [24] . The blade used NACA 0018 airfoil. It was assumed that the structural properties of the blades such as mass per unit length,

axial and bending stiffness. The blades, instead of struts are our concern [25]. The OC4 semi-submersible which was originally designed to support the NREL 5 MW wind turbine, was used to support the three bladed VAWTs. The design was carried out for a depth of 200 m. The same semi-submersible was used to support the 5MW Darrieus Deepwind rotor and Cheng et.al. (2015b) and Wang et. al. (2016). Due to difference in weight in the rotor mass, ballast water was adjusted to maintain the same draft. The properties of the semi-submersible were given below [25]:

Table 2.4: Principal parameter of the original semi-submersible

Parameter	Value
Water depth [m]	200
Draft of the platform [m]	20
Diameter at the mean water line (upper column/center column) [m]	10/6.5
Rotor mass, including blades, struts, tower and shaft [ton]	315.3
Center of mass of the rotor [m]	(0, 0, 48.14)
Platform mass including ballast and generator [ton]	13796.1
Center of mass for the platform [m]	(0, 0, -13.43)
Buoyancy at the equilibrium position [KN]	139816
Center of buoyancy [m]	(0, 0, -13.15)

2.3   Fixed VAWT model

One of the objective of this study, to carry out a comparative study with different VAWT model. Here, we used this model in our study to check the wind turbine performance parameter which will present in the next chapter. Right now, we just discuss the model. Beside to OC4 semi-submersible we used landbased VAWT. Three straight bladed fixed wind turbine is studied together with the OC4 new and old platform. The power output of the landbased wind turbine is 5 MW which used Darrieus rotor. The structural properties of straight bladed rotor such as structural properties of blades, struts, tower and shafts were determined based on DeepWind rotor (Vita, 2011) [25]. This turbine used NACA 0018 airfoil. The structural properties of the wind turbine are assumed to be same. The stiffness of the blades and struts were increased to avoid large deformation. The stiffness of the tower and shaft remained same. In a realistic situation, the stiffness of different component might differ slightly or might add additional struts as shown in the dashed line in the following figure [25].

As for the floating semi-submersible, we used similar configuration for old and new OC4 floater. They both support Darrieus 5 MW wind turbine. The figure added describes the arrangement of the wind turbine where the left one is the landbased wind turbine while the figure in the right side shows the arrangement of the OC4 semi-submersible both for the old and the new one. The layout of the optimized OC4 floater and original floater are similar.
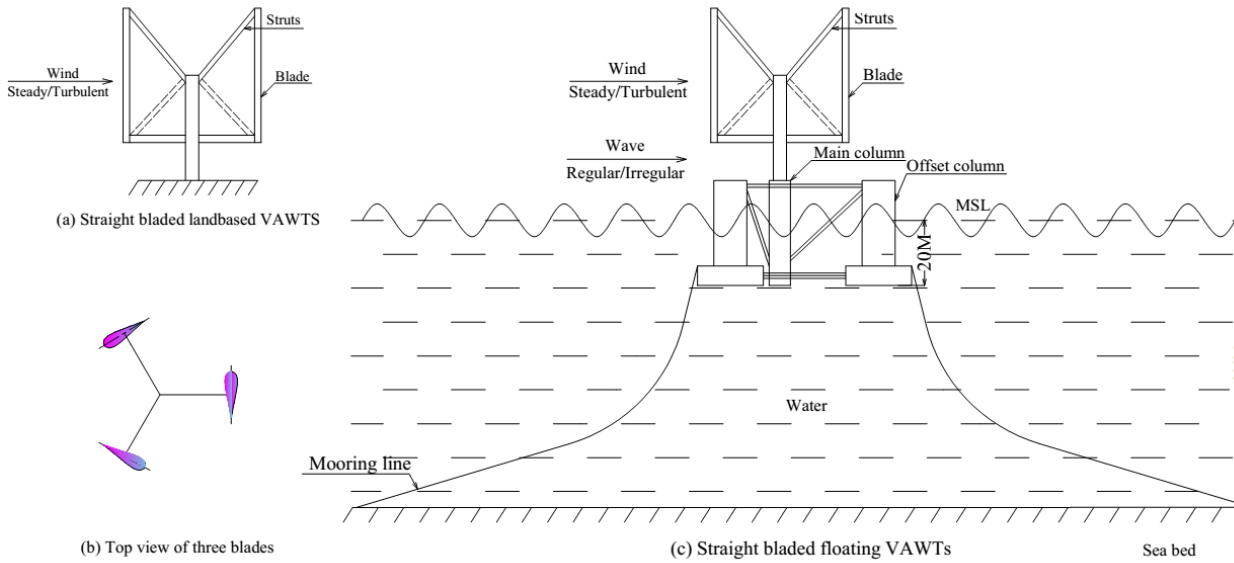
Figure 2.2: Schematic diagram of ladbased VAWT and OC4 floating VAWT

Table 2.5: Specification of landbased VAWT

Rated power [MW]	5.30
Rotor radius [m]	39.0
Rotor height [m]	80
Chord length [m]	2.7
Tower top height [m]	80.0
Aerofoil section	NACA 0018
Cut in, rated and cut out wind speed [m/s]	5.0, 14.0, 25.0
Rated rotor rotational speed [rpm]	1.08
Blade number	3

2.4 Coordinate system

The platform specifications refer to an inertial reference frame and platform DOFs. Three orthogonal set of axes X, Y and Z are chosen for this purpose. XY plane represent SWL and the remaining axis projected upward opposite to the gravity which coincide with the platform axis. The rigid body motion includes three translations and three rotations. Surge, sway and heave are linear displacement while roll, pitch and yaw are rotational motion. Positive surge defined as along the positive X axis, positive sway along the positive Y axis and positive heave along positive Z axis. Positive roll defined along positive X axis, pitch along Y axis and positive yaw along positive Z axis.

Figure 2.3: Coordinate system

2.5 Platform hydrodynamic properties

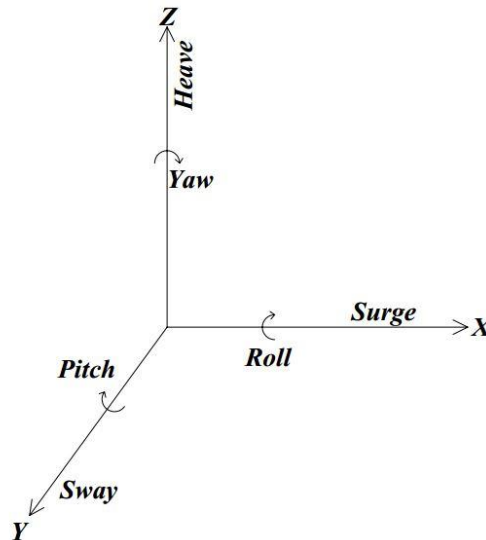Hydrodynamic loads include contribution from linear hydrostatics, linear excitation from incident waves, linear radiation from outgoing waves and non-linear effect such as drift forces[1]. In this study, we use linear theory of wave to solve the motion equation of the platform. According to this theory, the performance characteristics of the floating body can be described by the amplitude of the body as they are linearly related to each other. For this assumption, we can apply superposition of the effects. The hydrodynamic load on the platform are composed of three different contributions:

- Hydrostatic loads, which exists without any external forces such as wave or wind force. Buoyancy force which acts through the center of buoyancy according to the law of Archimedes and weight acting through the center of gravity creates a moment of magnitude $\triangle$.GZ. Here $\triangle$ is the weight displacement and GZ is the righting lever. Restoring force is also include in the calculation.
- Diffraction loads, corresponding to the loads on the body when the body is fixed in an oscillatory flow. Scattering wave forces and Froude-Krylov forces are closely related to this category.
- Radiation forces occurs when the when the body radiates waves in steady water in a frequency equals the applied frequency. They are known as added mass and damping of the floater.

2.5.1   Hydrostatic loads

The hydrostatic loads consists of restoring terms and the gravitational term acting along the Z axis. The total loads on the floating platform from linear hydrostatics,

$$F_i^{hydro} = \rho g V_0 \delta_{i3} - C_{ij}^{hydro} q_j \tag{2.1}$$

Where, ρ is the density of water, g is the gravitational acceleration, V_0 is the volume displacement of water, δ_{i3} is known as Kronecker-Delta function for (i,3) component. C_{ij}^{hydro} is the (i, j) component of from the linear hydrostatic restoring matrix from the effects of water plane area and the center of buoyancy and q_j is the Jth term of platform DOF[1]. The subscript value in equation (2.1) ranges from 1-6(1= surge, 2=sway, 3= heave, 4= roll, 5=pitch, 6= yaw) [23].

The first term in the right-hand side of the equation represents the buoyancy force derived from Archimedes principle which acted vertically upward and the magnitude is equal to the weight of the displaced water when the platform is in undisplaced position. Only the vertical component of heave is activated. The second term represents the net change in the hydrostatic forces and moments when the platform is displaced from its original position. The water density is taken as $1025\ kgm^{-3}$.

2.5.2   Hydrodynamics

The hydrodynamic loads associated with excitation forces which includes diffraction waves, radiated waves from the platform, added mass, viscosity, linear and nonlinear drags. In our study, we use potential flow theory, which helps us to formulate radiation and diffraction problem.

2.5.3   Potential flow theory

In this system, the flow around the bodies are treated as inviscid, incompressible and irrotational. This is because the viscous effects are limited to a thin layer next to the body called boundary layer. We can define the potential function, $\varphi(x, y, z, t)$ as a continuous function that satisfies the conservation of mass and momentum.

If $\varphi(x, y, z, t)$ is scalar quantity then,

$$\nabla \, X \, \nabla \varphi = 0 \tag{2.2}$$

And for irrotational flow,

$$\nabla \, X \, \bar{V} = 0 \tag{2.3}$$

Therefore, $V = \nabla \varphi$ and it satisfies the Laplace equation.

The linear potential problem is solved in HydroD by using WADAM in the frequency domain analysis. We had taken sixty components of the frequency and used a 3D panel model to solve the radiation and the diffraction problem. The solution regarding radiation problem, associated with oscillation of the platform is given in terms of frequency dependent added mass and damping matrices, A_{ij} and B_{ij}. The diffraction problem, consider hydrodynamic loads associated with the incident waves on the platform [23].

In GeniE, we first modelled our platform as a panel and then export the FEM files in the HydroD. In the first step, we check overall stability of the platform and then run the frequency domain analysis in WADAM. In the panel model, we adopt 1.2 m as the standard panel size. The semi-submersible was analyzed into a finite water depth 200 m.

The added mass and damping matrices has the dimension 6x6 for its six degrees of freedom. Due to the symmetry, the surge-surge elements of the frequency dependent added mass and damping matrices, A_{11} and B_{11} are identical to the sway-sway elements A_{22} and B_{22}. Likewise, the roll-roll elements A_{44} B_{44} are identical to the pitch-pitch elements, A_{55} and B_{55}. The behavior also exists for the wave heading angle. We get the same response at $0°, 120°$ and $240°$ wave headings. The layout of the design is shown below:
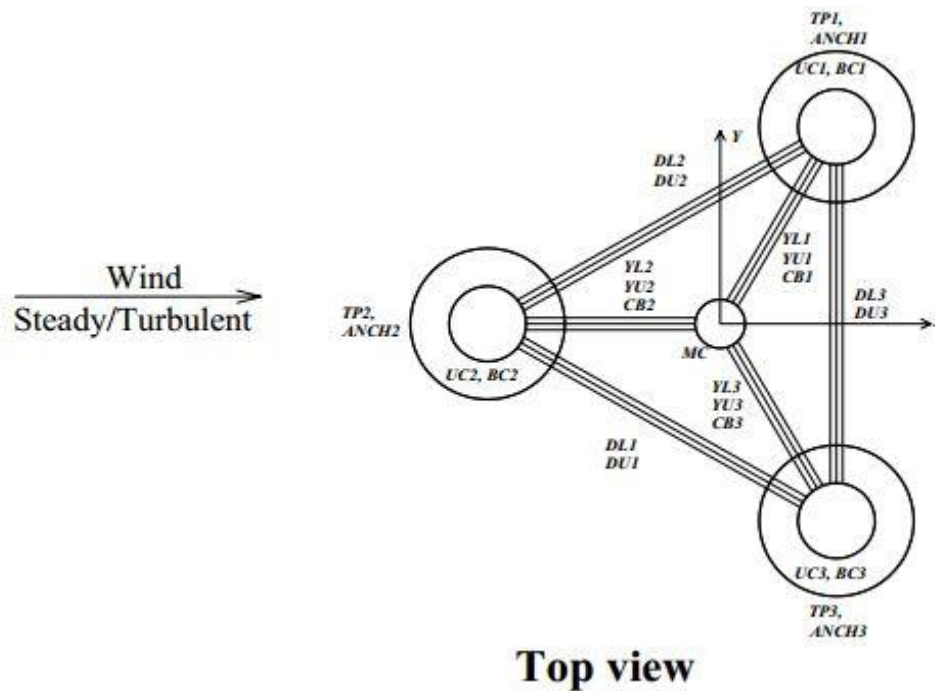

Figure 2.4: Wave heading direction with respect to platform

2.6 Morison's equation

Morison's formula is applicable for calculating the hydrodynamic loads on cylindrical structure when three points are fulfilled. They are:

- The diffraction effect is negligible.
- Radiation damping is negligible.
- Flow separation may occur.

The relative form of Morison's equation accounted form wave-induced excitation, radiation-induced added mass and flow separation induces viscous drag [23].

2.7 Added mass

Morison's law is a reasonable approximation for OC4 semi-submersible in most cases because diffraction effects are negligible in moderate to severe sea states, radiation damping in most cases is very small. In severe sea states, flow separation might occur is the upper part of the column [23]. For a cylinder in steady transverse flow, the Morison's equation can be expressed as[4]:

$$F = \frac{1}{2}C_d \rho D |u - u_r|(u - u_r) + \frac{1}{4}(1 + C_a)\rho \pi D^2 \dot{u} - \frac{1}{4}\rho C_a \pi D^2 \ddot{u}_r \qquad (2.4)$$

Here, ρ is the density of the fluid, D is the cylinder diameter, u and a_1 are the horizontal undisturbed velocity and acceleration at the midpoint of the strip. The mass and drag coefficients depends on Reynolds number, Keulegan-Carpenter number, surface roughness ratios and relative current number. The added mass coefficient C_a was selected such that $C_a \rho V$ is equaled the zero-frequency limit of A_{11} in the surge degree of freedom. The assumption for C_a is independent of the depth and the motion is relatively in the low frequency region. u_r is the cylinder velocity.

For the platform, we use three base columns as heave plate. The force on a heave plate need to model carefully because the heave plate does not scale proportionally with respect to the displaced fluid. The hydrodynamic force on heave plate is to be modelled according to the modified Morison's equation which mentioned below [23]:

$$F = \frac{1}{2}C_{dz} \rho A_c |w - u_r|(u - u_r) + \rho C_{az} V_r (\dot{w} - \dot{u}_r) + \frac{1}{4}\pi D_h^2 p_b - \frac{1}{4}\pi (D_h^2 - D_c^2)p_t \qquad (2.5)$$

Where, C_{dz} is drag coefficient in the heave direction, A_c is the cross-sectional area of the base column, w is the wave particle velocity and u_r is heave velocity of the base column. C_{az} is the added mass coefficient, V_r is the reference heave volume, $\dot{w}$ is the vertical wave particle acceleration, $\dot{u}_r$ is the vertical acceleration of the base column, D_h is the diameter of the base column, D_c is the diameter of the upper column and p_b, p_t are the dynamic pressure acting on the bottom and top faces of the column. The first term represents the drag force in the heave direction, the second one stands for added mass force and the last two part represents the Froude-Krylov

force expressed in terms of pressure. The table shown below essentially summarizes the hydrodynamic properties of the floating platform:

Table 2.6: Hydrodynamic coefficients

Water density (ρ)	$1025\ kgm^{-3}$
Water depth (h)	200 m
Dispalced water in undisplaced position (V_0)	9857.6 ton
Added mass coefficient for all members (C_a)	0.63
Drag coefficient for main column (C_d)	0.56
Drag coefficient for upper column (C_d)	0.61
Drag coefficient for base column (C_d)	0.68
Drag coefficient for braces and pontoon (C_d)	0.63
Drag coefficient for base column (C_{dz})	4.80

2.8 Intact Floating Stability

Floating stability implies a stable equilibrium and reflection of total integrity against downflooding and capsizing. Satisfactory floating stability for wind turbine units is necessary to support the safety level required for the involved structures. The intact stability of the structure is discussed below:

- The wind heeling moment applied in the stability calculation for a wind speed equal to the wind speed that produces the largest rotor thrust assuming the that the rotor plane is normal to the direction of flow.
- For sufficient stability, also in fault situation that the turbine does not yaw out of the wind during severe storm conditions, it will be necessary to assume that the rotor plane is perpendicular to the wind when calculating the wind heeling moment. A wind speed of 36 m/s may be assumed for this situation.
- The area under the righting moment curve to the second intercept or down-flooding angle, whichever is less, shall be equal or greater than 140% of the area under the wind heeling moment curve to the same limiting angle [26].
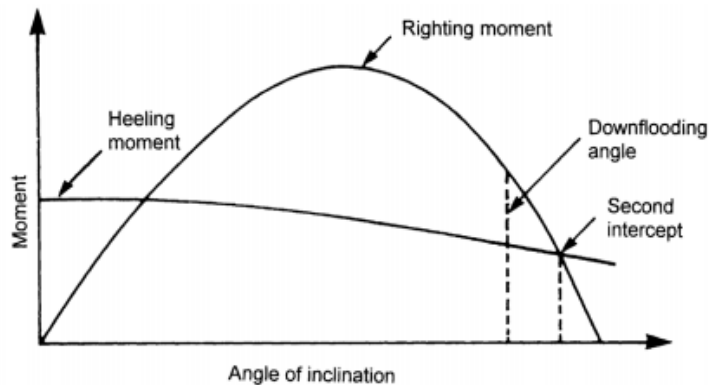

Figure 2.5: Righting moment and wind heeling moment curves

openings. The heeling moment is determined for the maximum thrust force, obtained at the rated wind speed, given by the following equation:

$$M_{wind} = F_{T,rated} \, l \, cos^2\theta$$
$$= \frac{1}{2}\rho_{air} \, \frac{D_{rotor}^2}{4} \, \pi \, C_T \, v_{rated}^2 \, l \, cos^2\theta$$

(2.6)

The lever arm l is the distance between the force application point, taken at the hub, at the point of rotation. For column stabilized units such as semi-submersibles, the area under the righting moment curve to the angle of downflooding shall be equal to or greater than 130% of the area under the wind heeling moment curve to the same limiting angle.

2.9   Modelling in SIMO

To develop a time domain simulation, we used a couple analysis tool SIMO-RIFLEX-AC. The floating body is developed in SIMO. At first, the FEM body is used as a panel model in HydroD. Then we use WADAM and carried out the frequency domain analysis. The resulting file is then converted into system description file. There we modify some parameter such as buoyancy compensation, applied force, center of gravity of the platform and fixing the value for slender elements.

2.10   Modifying parameters in SIMO

SIMO-RIFLEX is used for coupled analysis of the system in which the platform is used modelled as rigid body and the mooring lines as RIFLEX elements. Restoring matrix and transfer function can be obtained from the panel analysis.

So when we transfer the definition of the body in SIMO we need to modify some parameters due to some internal inconsistency in these two software. IN SIMO, the floating platform excluding the RIFLEX elements is neutrally buoyant. But it is not the case. Similar thing happens for the restoring matrix. In SIMO, the effect of gravity force and buoyancy is considered through the restoring matrix. But RIFLEX uses this force as nodal forces as it uses finite element method. To address this inconsistency, we need to adjust the buoyancy compensation force (Kvittem, 2014).

Now modelling in SIMO, there will be a moment acting on the body. But this force is cancelled by the gravity force. Overall, an inconsistent static configuration arises in the analysis. In case of dynamic analysis, it gives a strenuous restoring moment (Kvittem, 2014).

 In the corrected model, we apply an upward force through the center of buoyancy and downward through the center of gravity. These forces gives rise restoring forces since they act in the global direction. But they are included in the WADAM analysis. So, we need to subtract this part from

the restoring matrix. This method effectively then includes only the water plane stiffness. The procedure is described below:

1. In the Simo description file, we modified the following things:
   - In the 'BODY MASS DATA' section, we used the COG value of the platform without considering wind turbine.
   - In the 'MASS COEFFICIENTS' section, we used the COG value of the platform without considering wind turbine.
   - In the 'LINEAR STIFFNESS MATRIX' SECTION I used the following formula:

$$
\begin{aligned}
C_{44}^{new} &= C_{44}^{wadam} - \rho g V_0 z_b + m g z_g = \mathbf{1110729.768} \\
C_{55}^{new} &= C_{55}^{wadam} - \rho g V_0 z_b + m g z_g = \mathbf{1110729.768} \\
C_{46}^{new} &= C_{46}^{wadam} - \rho g V_0 x_b + m g x_g = C_{46}^{wadam} \\
C_{56}^{new} &= C_{56}^{wadam} - \rho g V_0 x_b + m g x_g = C_{56}^{wadam}
\end{aligned}
\tag{2.7}
$$

   where V_0 is the displaced volume of the body (platform), m is the mass of the platform with turbine, $(x_b, y_{b,} z_b)$ are the buoyancy location in the global coordinate system and $(x_g, y_{g,} z_g)$ are center of gravity location in the global coordinate system.

2. In the specified force section, we modified the following things:
   - 'Gravity of the floater without the brace' section we consider the mass of the platform and then multiplied with 9.80665 which gives **93578 KN**.
   - 'Buoyancy of the floater without the brace' section we consider the buoyancy of the whole body (Platform+Turbine). The buoyancy force is **96670.516 KN.**

2.11 Equation of motion and natural periods

Applying Newton's second law and considering the applied load, the equation of motion for a floating object is given by:

$$
F_i e^{-i\xi t} = \sum_{j=1}^{6} \left[(M_{ij} + A_{ij}) \frac{d^2 \eta_j}{dt^2} + B_{ij} \frac{d\eta_j}{dt} + C_{ij} \eta_j \right] (i = 1 - 6)
\tag{2.8}
$$

The left term in the equation, represents the external exciting force say wave induced loads or wind loads. M_{ij} is the mass matrix and the body is symmetric about the XZ plane. So, the mass matrix is given in the following form:

$$M_{ij} = \begin{bmatrix} M & 0 & 0 & 0 & Mz_G & 0 \\ 0 & M & 0 & -Mz_G & 0 & 0 \\ 0 & 0 & M & 0 & 0 & 0 \\ 0 & -Mz_G & 0 & I_x & 0 & -I_{xz} \\ Mz_G & 0 & 0 & 0 & I_y & 0 \\ 0 & 0 & 0 & -I_{xz} & 0 & I_z \end{bmatrix}$$

The term A_{ij}, B_{ij} and C_{ij} are known as added mass, damping coefficients and restoring coefficients respectively. By imposing the relation $\eta_i = \bar{\eta}_i e^{-i\xi t}$, the equation of motion is given by:

$$(A_{ii} + M_{ii})\frac{d^2\bar{\eta}_i}{dt^2} + B_{ii}\frac{d\bar{\eta}_i}{dt} + C_{ii}\bar{\eta}_i = F_i \quad (i = 1 - 6) \tag{2.9}$$

In this simplification, we assume the body oscillates at same wave amplitude and frequency at every instant and the coupling effect is disregarded. So, the natural period of a floating body for an undamped system is given by:

$$T_{ni} = 2\pi \sqrt{\frac{M_{ii} + A_{ii}}{C_{ii}}} \quad (i = 1 - 6) \tag{2.10}$$

This is the basic formula to calculate the natural frequency of the platform when turbine is in the parked condition. We evaluate the natural period by performing a decay test. The description is given below.

2.12   Stability of the Semi-submersible

The design is optimized for the following parameter. The diameter of the base column is 20 m, diameter of the upper column is 10 m and the center to center distance from column to column is 52 m. The final moment curve is shown in the figure 2.6. The heeling moment curve is a straight line and the contribution came from the external force such as air and water or from within the structure. The heeling moment for our analysis was 53880000 N-m. The second one is known as restoring moment of the structure. It is the ability for the structure to regain its original position. The first intercept point is 5.2 degrees and the second intercept is 112 degrees. In our design our maximum allowable angle for the first intercept is 7 degrees.
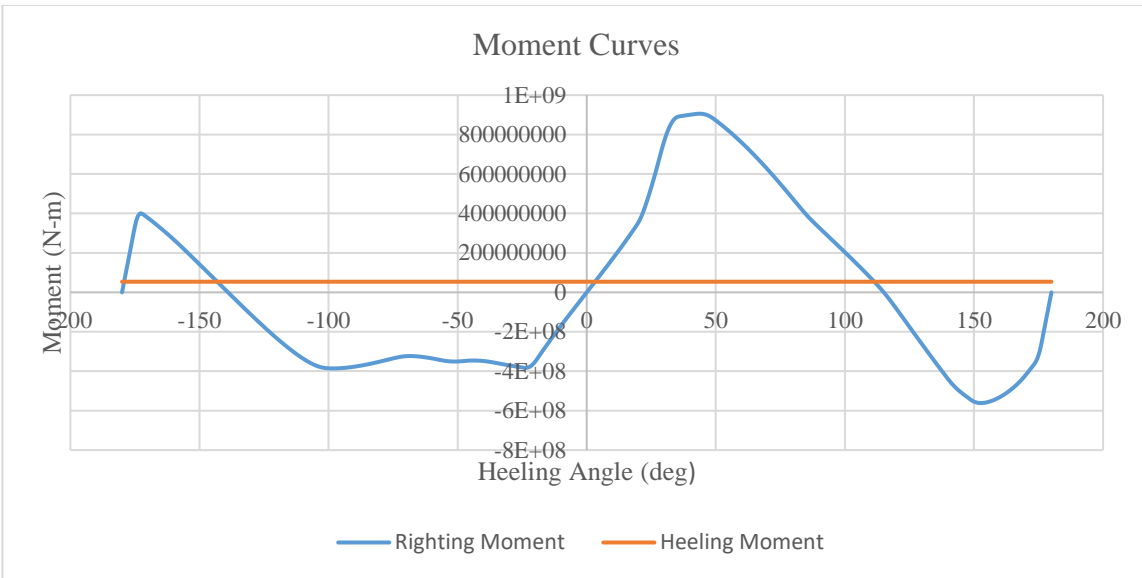
Figure 2.6: Moment curve

Reducing the diameter results an increase of intercept angle. We make an estimation of the intercept angle compared to the diameter of the column. As the diameter of the two column increases the intercept angle decreases. The lowest allowable angle of intercept occurs at 19 m diameter. But considering other situation, we choose 20 m as the base column diameter. Another requirement for the moment curve that area enclosed by the curve is greater than 140% of the total area under the heeling moment curve. So, we can easily estimate that this condition is also satisfied. All the requirements stipulated by the DNV is satisfied.
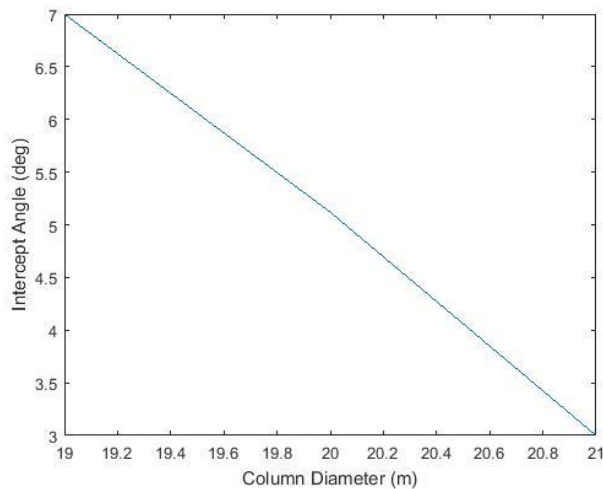

Figure 2.7: Change of intercept angle by changing draft

Above we discussed about the new OC4 semi-submersible which we optimized based on the concept of OC4 semi-submersible design to support the NREL 5 MW wind turbine. Some of the

analysis was carried out in my project work. The OC4 semi-submersible is optimized on the basis of following parameters such as weight and principal parameters without altering the behavior of the sei-submersible. We are able to reduce the weight significantly and designed in a way which cleverly adjust the natural frequency outside the range of wave excitation.

Chapter 3

Aerodynamic & Hydrodynamic loads on VAWT

3.1   Overview of Aerodynamic Models for FVAWT

A variety of aerodynamic model has been proposed by different researcher to calculate the aerodynamic loads on VAWTs. These includes actuator cylinder (AC) flow model, streamtube models which consists single streamtube model, double streamtube model, multi streamtube model, vortex model, computational fluid dynamics model. In this study, for our analysis we used AC model which is primarily developed by Madsen et al. [17] and the further development was carried out by Cheng et al. [27].
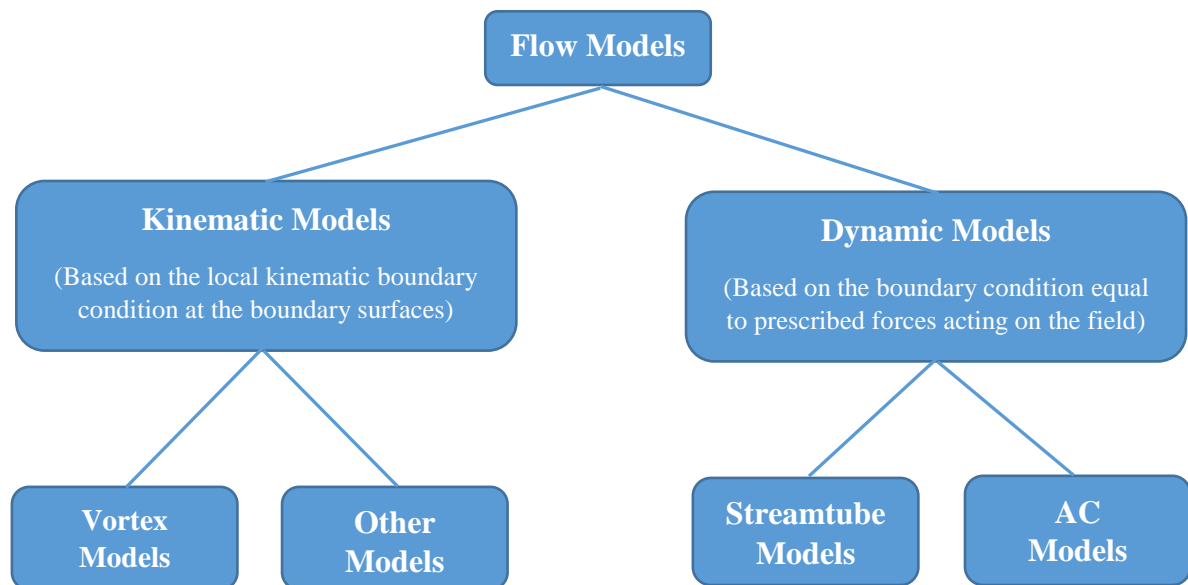

Figure 3.1: Flow chart of different aerodynamic model (Taken from Madsen 1982)

3.2   The Actuator Cylinder Flow Model

The AC model was first developed from the PhD study carried by Madsen et al. [17]. The basic idea to use the known AD (Actuator Disc) flow model from HAWT and to develop a general approach of an actuator surface coinciding with the swept area of the actual turbine [17]. For a straight bladed VAWT the swept surface area is cylindrical. To reduce the complexity of the model this model is a 2D representation of the general model.

The AC model is a quasi-static Eulerian model. The normal and the tangential forces Q_n and Q_t resulting from the blade forces are applied on the flow as volume force perpendicular and tangential to the rotor plane as shown in the figure 3.2.
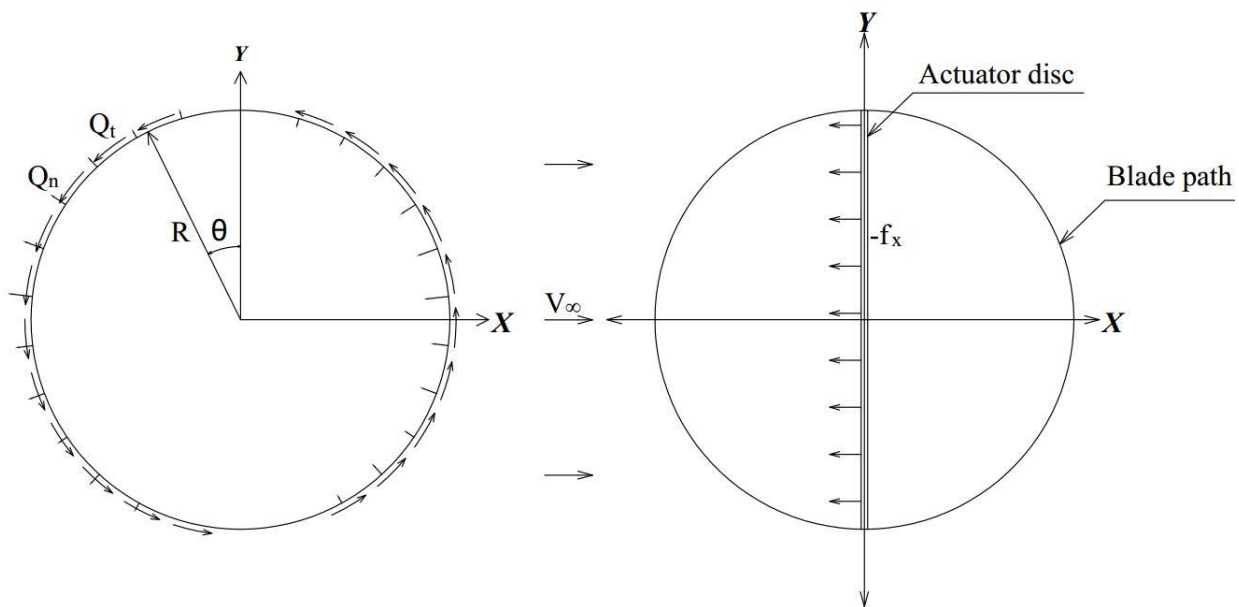

Figure 3.2: Actuator cylinder model [24]

Our task is to determine the flow field under the disturbance of the external volume forces. The volume forces f_x, uniform and parallel to the free stream velocity V_∞. If the drag force is D per unit length and the velocity, $V_\infty(1-a)$, then applying momentum theory [17],

$$D = 2 \text{ x2R x } \rho V_\infty^2 (1 - a)a \tag{3.1}$$

And the drag force D and f_x are connected by

$$\lim_{n \to 0} \int_{-n}^{n} f_x \, dx = 2R . Q_x = \text{-D} \tag{3.2}$$

From eq. (2) a pressure jump $\triangle p$, when passing through the disc, where $\triangle p$ is given by,

$$\Delta p = \frac{D}{2R} = -Q_x$$

Radial volume forces are distributed on a cylindrical surface and will thus create a pressure jump, $\triangle p$ across the surface.

$$\Delta p = \lim_{n\to 0} \int_{R-n}^{R+n} f_r(\theta)\, dr = Q_r(\theta) \tag{3.3}$$

The power extracted from the fluid per unit length of the cylinder is given by

$$P_{ideal} = \int_0^{2\pi} V_r(\theta).\Delta p(\theta).Rd\theta \tag{3.4}$$

And the power coefficient is given by

$$C_{p,ideal} = \frac{P}{\frac{1}{2}\,\rho V_\infty^3.2R} = \frac{\int_0^{2\pi} V_r(\theta).\Delta p(\theta).Rd\theta}{\frac{1}{2}\,\rho V_\infty^3.2R} \tag{3.5}$$

Finally, the extracted power by the turbine and its power coefficient are defined by the following equations

$$P = \frac{1}{2\pi}\int_0^{2\pi} N\, F_t(\theta).\Omega.Rd\theta \tag{3.6}$$

and

$$C_p = \frac{P}{\frac{1}{2}\,\rho V_\infty^3.2R} = \frac{\frac{1}{2\pi}\int_0^{2\pi} N\, F_t(\theta).\Omega.Rd\theta}{\frac{1}{2}\,\rho V_\infty^3.2R} \tag{3.7}$$

3.2.1 Governing equations and method of solution

The basic equations and solution method described by Madsen et al. [17] will be described briefly. The basic equation for the 2D case is the Euler equation. Suppose the velocity components are v_x and v_y can be written as,

$$v_x = 1 + w_x \text{ and } v_y = w_y \tag{3.8}$$

Now the Euler equations takes the form:

$$\frac{\partial w_x}{\partial x} + w_x\frac{\partial w_x}{\partial x} + w_y\frac{\partial w_x}{\partial y} = -\frac{\partial p}{\partial x} + f_x \tag{3.9}$$

$$\frac{\partial w_y}{\partial x} + w_x\frac{\partial w_y}{\partial x} + w_y\frac{\partial w_y}{\partial y} = -\frac{\partial p}{\partial y} + f_y \tag{3.10}$$

and the continuity equation is given by

$$\frac{\partial w_x}{\partial x} + \frac{\partial w_y}{\partial y} = 0 \tag{3.11}$$

Where p is the pressure and f is the volume forces.

The value of $Q_n(\theta)$ and $Q_t(\theta)$ derived from the blade forces per unit length by the following equations:

$$Q_n(\theta) = \frac{BF_n\,\theta}{2\pi R\rho V_\infty^2} \tag{3.12}$$

$$Q_t(\theta) = \frac{BF_t\,\theta}{2\pi R\rho V_\infty^2} \tag{3.13}$$

Where B is the blade number and R is the radius of blade path.

Equation (9) and (10) can be rewritten as:

$$\frac{\partial w_x}{\partial x} = -\frac{\partial p}{\partial x} + f_x + g_x$$

$$\frac{\partial w_x}{\partial y} = -\frac{\partial p}{\partial y} + f_y + g_y \tag{3.14}$$

Where g_x and g_y are second order forces:

$$g_x = -(w_x \frac{\partial w_x}{\partial x} + w_y \frac{\partial w_x}{\partial y})$$

$$g_y = -(w_x \frac{\partial w_y}{\partial x} + w_y \frac{\partial w_y}{\partial y}) \tag{3.15}$$

So, the final equation for the pressure:

$$\frac{\partial^2 p}{\partial x^2} + \frac{\partial^2 p}{\partial y^2} = (\frac{\partial f_x}{\partial x} + \frac{\partial f_y}{\partial y}) + (\frac{\partial g_x}{\partial x} + \frac{\partial g_y}{\partial y}) \tag{3.16}$$

Which is Poisson type equation.

The solution of this equation with the appropriate boundary conditions $p \to 0$ and $x, y \to \infty$ can be written as:

$$p(f) = \frac{1}{2\pi} \iint \frac{f_x(x-\xi) + f_y(y-\eta)}{(x-\xi)^2 + (y-\eta)^2} \, d\xi d\eta \tag{3.17}$$

$$p(g) = \frac{1}{2\pi} \iint \frac{g_x(x-\xi) + g_y(y-\eta)}{(x-\xi)^2 + (y-\eta)^2} \, d\xi d\eta \tag{3.18}$$

Once the pressure field is found the velocities can be determined by equation 3.19 and 3.20.

$$w_x = -p(f) + If_x - p(g) + Ig_x = w_x(f) + w_x(g) \tag{3.19}$$

$$w_y = \iint_{-\infty}^{x} \frac{\partial}{\partial x} p(f) dx' + If_y - \iint_{-\infty}^{x} \frac{\partial}{\partial y} p(g) dx' + Ig_y = w_x(f) + w_x(g) \tag{3.20}$$

Where, $If_x = \int_{-\infty}^{x} f_x dx'$

$$If_y = \int_{-\infty}^{x} f_y dx'$$

$$Ig_x = \int_{-\infty}^{x} g_x dx'$$

$$Ig_y = \int_{-\infty}^{x} g_y dx'$$

The final solution can be written as a sum of two parts. One is linear and the other part is nonlinear. An important characteristic for the solution as the prescribed forces only applied on a circle, so the pressure solution for the linear part become the solution of Laplace equation in two connected regions; outside the cylinder and inside the cylinder[8].

3.2.2 Linear Solution

For the normal loading on the AC which is the largest force than tangential force, the linear solution can be worked out [27]:

$$
\begin{aligned}
w_x = &-\frac{1}{2\pi} \int_0^{2\pi} Q_n(\theta) \frac{-(x+\sin\theta)\sin\theta+(y-\cos\theta)\cos\theta}{(x+\sin\theta)^2+(y-\cos\theta)^2} d\theta - \\
&\frac{1}{2\pi} \int_0^{2\pi} Q_t(\theta) \frac{-(x+\sin\theta)\cos\theta-(y-\cos\theta)\sin\theta}{(x+\sin\theta)^2+(y-\cos\theta)^2} d\theta - \left(Q_n \left(\cos^{-1} y\right)\right)^* + \\
&\left(Q_n \left(-\cos^{-1} y\right)\right)^{**} - \left(Q_t \left(\cos^{-1} y\right)\frac{y}{\sqrt{1-y^2}}\right)^* - \left(Q_t \left(-\cos^{-1} y\right)\frac{y}{\sqrt{1-y^2}}\right)^{**}
\end{aligned}
\tag{3.21}
$$

$$
\begin{aligned}
w_y = &-\frac{1}{2\pi} \int_0^{2\pi} Q_n(\theta) \frac{-(x+\sin\theta)\cos\theta+(y-\cos\theta)\sin\theta}{(x+\sin\theta)^2+(y-\cos\theta)^2} d\theta \\
&-\frac{1}{2\pi} \int_0^{2\pi} Q_t(\theta) \frac{(x+\sin\theta)\sin\theta-(y-\cos\theta)\cos\theta}{(x+\sin\theta)^2+(y-\cos\theta)^2} d\theta
\end{aligned}
\tag{3.22}
$$

The term marked with * in equation 3.21 shall be added inside the cylinder and in case wake behind the cylinder both the term marked with * and ** shall be included. It is to be noted that the original work of Madsen et al. [17] does not include the tangential terms but in the work of Cheng et al. [27] this term is included.

Linear solution

Assuming the loading is piecewise constant we can derive from equation (3.21) and (3.22):

$$w_x = -\frac{1}{2\pi}\sum_{i=1}^{i=N} Q_{n,i} \int_{\theta_i-\frac{1}{2}\Delta\theta}^{\theta_i+\frac{1}{2}\Delta\theta} \frac{-(x+\sin\theta)\sin\theta + (y-\cos\theta)\cos\theta}{(x+\sin\theta)^2 + (y-\cos\theta)^2} d\theta$$

$$-\frac{1}{2\pi}\sum_{i=1}^{i=N} Q_{t,i} \int_{\theta_i-\frac{1}{2}\Delta\theta}^{\theta_i+\frac{1}{2}\Delta\theta} \frac{-(x+\sin\theta)\cos\theta + (y-\cos\theta)\sin\theta}{(x+\sin\theta)^2 + (y-\cos\theta)^2} d\theta \qquad (3.23)$$

$$w_y = -\frac{1}{2\pi}\sum_{i=1}^{i=N} Q_{n,i} \int_{\theta_i-\frac{1}{2}\Delta\theta}^{\theta_i+\frac{1}{2}\Delta\theta} \frac{-(x+\sin\theta)\cos\theta + (y-\cos\theta)\sin\theta}{(x+\sin\theta)^2 + (y-\cos\theta)^2} d\theta$$

$$+\frac{1}{2\pi}\sum_{i=1}^{i=N} Q_{t,i} \int_{\theta_i-\frac{1}{2}\Delta\theta}^{\theta_i+\frac{1}{2}\Delta\theta} \frac{-(x+\sin\theta)\sin\theta + (y-\cos\theta)\cos\theta}{(x+\sin\theta)^2 + (y-\cos\theta)^2} d\theta \qquad (3.24)$$

Where N is the total number of calculation points, $\Delta\theta = \frac{2\pi}{N}$ and $\theta_i = \frac{\pi}{N}(2i-1)$ for $i = 1,2,3\,.....N$.

Only the induced velocity at the cylinder are of concern, the total velocity solution at calculation point (x_j, y_j) on the cylinder can then be written as:

$$w_{x,j} = -\frac{1}{2\pi}\left(\sum_{i=1}^{i=N} Q_{n,i}I_{1,i,j} + \sum_{i=1}^{i=N} Q_{t,i}I_{2,i,j}\right) - \left(Q_{n,N+1-j}\right)^* - \left(Q_{t,N+1-j}\frac{y_j}{\sqrt{1-y_j^2}}\right)^* \qquad (3.25)$$

$$w_{x,j} = -\frac{1}{2\pi}\left(\sum_{i=1}^{i=N} Q_{n,i}I_{2,i,j} + \sum_{i=1}^{i=N} Q_{t,i}I_{1,i,j}\right) \qquad (3.26)$$

Where the terms marked with * in equation (25) and (26) are only added for $j = \frac{N}{2}$

$I_{1,i,j}$ and $I_{2,i,j}$ are influenced coefficients in point j influenced by another point I are given by

$$I_{1,i,j} = \int_{\theta_i-\frac{1}{2}\Delta\theta}^{\theta_i+\frac{1}{2}\Delta\theta} \frac{-(x_j+\sin\theta)\sin\theta + (y_j-\cos\theta)\cos\theta}{(x_j+\sin\theta)^2 + (y_j-\cos\theta)^2} d\theta \qquad (3.27)$$

$$I_{2,i,j} = \int_{\theta_i-\frac{1}{2}\Delta\theta}^{\theta_i+\frac{1}{2}\Delta\theta} \frac{-(x_j+\sin\theta)\cos\theta + (y_j-\cos\theta)\sin\theta}{(x_j+\sin\theta)^2 + (y_j-\cos\theta)^2} d\theta \qquad (3.28)$$

Where $x_j = -\sin(j\Delta\theta - \frac{1}{2}\Delta\theta)$, $y_j = \cos(j\Delta\theta - \frac{1}{2}\Delta\theta)$

3.2.3 Modified Linear Solution

To compute the non-linear solution directly, it takes time. To make the solution in better agreement with the non-linear solution, a correction was proposed by Madsen et al. [17]. Madsen suggested to multiply the velocities from the linear solution w_x and w_y with the factor:

$$K_a = \frac{1}{1-a}$$

But according to Cheng et al. [27] that the correction proposed by Madsen et al. can give some deviation in the power coefficient at high tip speed ratios when compared to the experimental data. The modified K_a:

$$K_a = \begin{cases} \dfrac{1}{1-a}, & a \leq 0.15 \\ \dfrac{1}{1-a}(0.65 + 0.35\exp(-4.5(a-0.15))), & a > 0.15 \end{cases}$$

3.3 Dynamic Stall model

Dynamic stall is a flow phenomenon that involves large scale unsteady viscous effects. Although the yawed flow on the rotor blade have influence, the fundamental behavior is contained in the two-dimensional problem [28]. This event is evident for wind turbine as confirmed from the measurements of aerodynamic coefficients. There are different models that attempts to describe this phenomenon. But in this study, we use Beddoes-Leishman dynamic stall model (1989).

This model is a semi empirical model that is used to describe the indicial response. Two force coefficients arise from the indicial response. They are normal force coefficient (C_N) and the other is moment force coefficient (C_M). The indicial response is derived from the linearized differential equations for an unsteady, inviscid and compressible fluid. The increment in C_N due to a step change in angle of attack ($\triangle\alpha$) can be divided into non-circulatory component (C_N^l) and a circulatory component (C_N^c). There are expressed as follows [29]:

$$\Delta C_N^c = C_{N\alpha}\phi_\alpha^c \Delta\alpha$$

$$\Delta C_N^l = \frac{4}{M}\phi_\alpha^l \Delta\alpha$$

(3.29)

Where, $C_{N\alpha}$ is the normal force coefficient curve slope, M is the Mach number, ϕ_α^l is the non-circulatory indicial function and ϕ_α^c is the circulatory indicial function. The calculated attached flow response is modified based on the effective flow separation point on the low-pressure side of the airfoil. The separation point is given by the function $f = \frac{x}{c}$ where c is the chord length and x is the measured distance from the leading edge. An approximation used by Beddoes based on Kirchhoff theory which relates C_N and C_c to the flow separation is given by the formula.

$$C_N = C_{N\alpha}(\alpha - \alpha_0)\left(\frac{1 + \sqrt{f}}{2}\right)^2 \tag{3.30}$$

$$C_c = C_{N\alpha}(\alpha - \alpha_0)\tan(\alpha)\sqrt{f}$$

Where, α is the angle of attack and α_0 is the zero angle of attack [29].

The final component of the model represents the vortex buildup and shedding that occurs during dynamic stall. Vortex lift can be modelled as an excess circulation in the vicinity of the airfoil. The magnitude of the increased lift can be found from the difference of the attached flow (C_N) and the the attached flow obtained from Kirchhoff law [29]. Due to the effect of vortex component, the chordwise force coefficient is defined by the following equation [21].

$$C_c = C_{N\alpha}(\alpha_e - \alpha_0)\alpha_e\sqrt{f_c''} + C_N^v \alpha_e(1 - \tau_v) \tag{3.31}$$

Where α_e is the effective angle of attack, α_0 is the zero-lift angle, $C_{N\alpha}$ is the normal force coefficient slope curve, f_c'' is the dynamic separation point function, C_N^v is the normal force coefficient from vortex lift contribution and τ_v is non-dimensional parameter to track the position of the vortex across the airfoil. The drag and lift coefficient is given by the following equation [29].

$$C_L = C_N \cos(\alpha) + C_c \sin(\alpha) \tag{3.32}$$

$$C_D = C_N \sin(\alpha) - C_c \cos(\alpha) + C_{d0} \tag{3.33}$$

Here, C_{d0} is the minimum drag coefficient to the zero angle of attack.

The accumulation of AC method and the Beddoes-Leishman dynamic stall model is shown in the flow chart.

3.4   Method of analysis

In this study, actuator cylinder model (AC), developed by Madsen et al. (1982) and which was modified by Cheng et al. (2016a) was used to determine various wind loads. This model is used to design three straight bladed VAWTs and a corresponding generator-torque controller. AC model predicts more accurately different aerodynamic loads than DMS method provided with similar computational efficiency. The code SIMO-RIFLEX-AC developed by Cheng et al.(2016b) was used to conduct fully coupled analysis. The flow chart for a floating VAWTs using the AC method is shown below. For each time step, the induced velocity is calculated according to the AC method. The effect of dynamic stall is also included in the calculation by using the Beddoes-Leishman dynamic stall model. The effect of wind shear and turbulence can also be accounted if there is any local free wind speed.
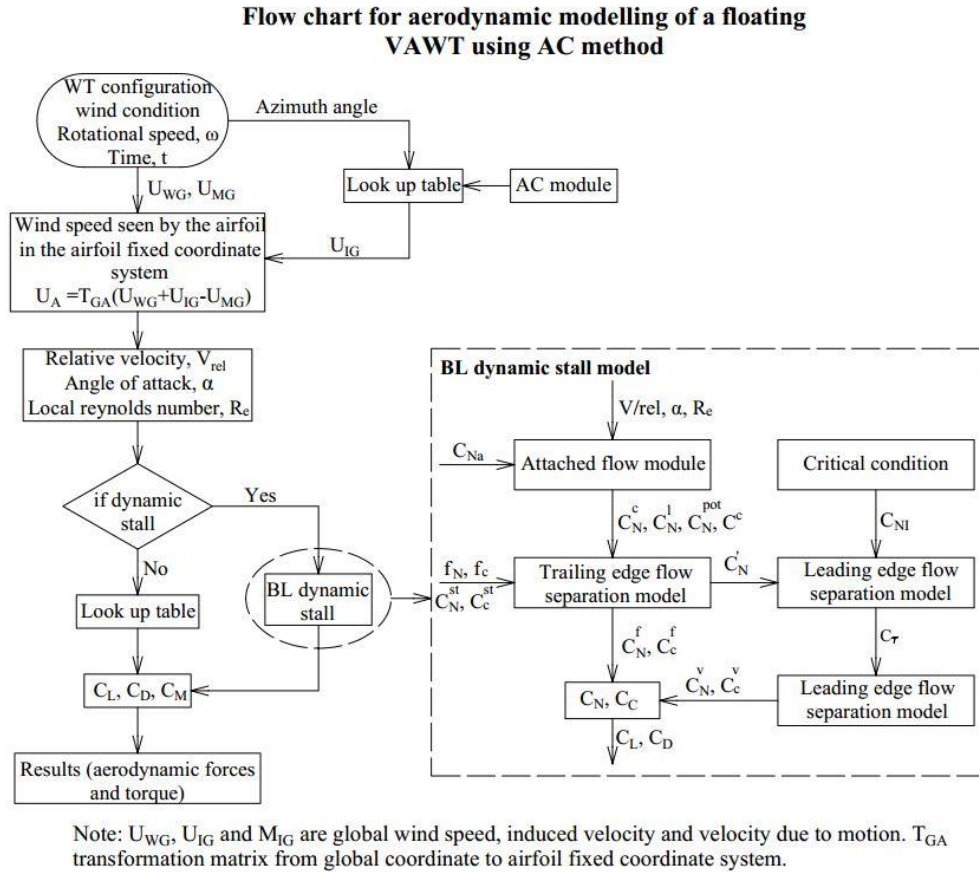
Flow chart for aerodynamic modelling of a floating VAWT using AC method

Note: U_{WG}, U_{IG} and M_{IG} are global wind speed, induced velocity and velocity due to motion. T_{GA} transformation matrix from global coordinate to airfoil fixed coordinate system.

Figure 3.3: Flow chart of modelling of VAWT using AC method [21]

3.5 Coupled model for FVAWT

The code developed for AC model by Cheng et al. [21] then integrated with SIMO-RIFLEX to get the fully coupled aero-hydro-servo-elastic code, namely SIMO-RIFLEX-AC for numerical modelling and time domain simulation of FVAWT. SIMO and RIFLEX was originally developed by MARINTEK and widely used in the offshore oil gas industry. SIMO is capable to calculate the rigid body hydrodynamics forces and different moments on the floater which is designed to support the VAWT. RIFLEX is used to model the tower, blades, struts, mooring lines as flexible finite elements and provides a link with the AC code. The AC code is used to account the total aerodynamic load acting on the wind turbine. Generator torque characteristic was written in Java. An external Dynamic Link Library (DLL) passes information from RIFLEX to AC and from AC to RIFLEX. The force calculation is done in each time step. Together this codes provides a coupled aero-hydro-servo-elastic simulation tool with complicated hydrodynamic analysis, nonlinear FEM solver, aerodynamic solver and user defined control strategy.

In our study, a OC4 semi-submersible supporting a straight bladed VAWT was considered. The aerodynamic loads acting on the blades can be accounted by the application of AC model. The effect of wind turbulence, dynamic stall was considered. But the effect of tip loss and drag forces on the tower is neglected [21].

In case of structural model, the semi-submersible represents a rigid body. The tower, blades and shaft was designed as nonlinear beam elements. The mooring ropes are designed as nonlinear bar elements as they only contribute the axial force in the global structure. The dynamic equation then solved in the time domain by using Newmark-β integration method [21].

To account the hydrodynamic forces on the semi-submersible we built a model in GeniE and then analyze in the frequency domain by HydroD and then transfer the system description file in SIMO. The hydrodynamic model is a combination of potential flow and Morrison's model. Added mass, damping and first order wave excitation were obtained from potential flow theory. Morrison's formula was applied to account the viscous damping and to the braces and mooring lines that is not included in the potential flow. A flow chart is shown in figure 3.4:
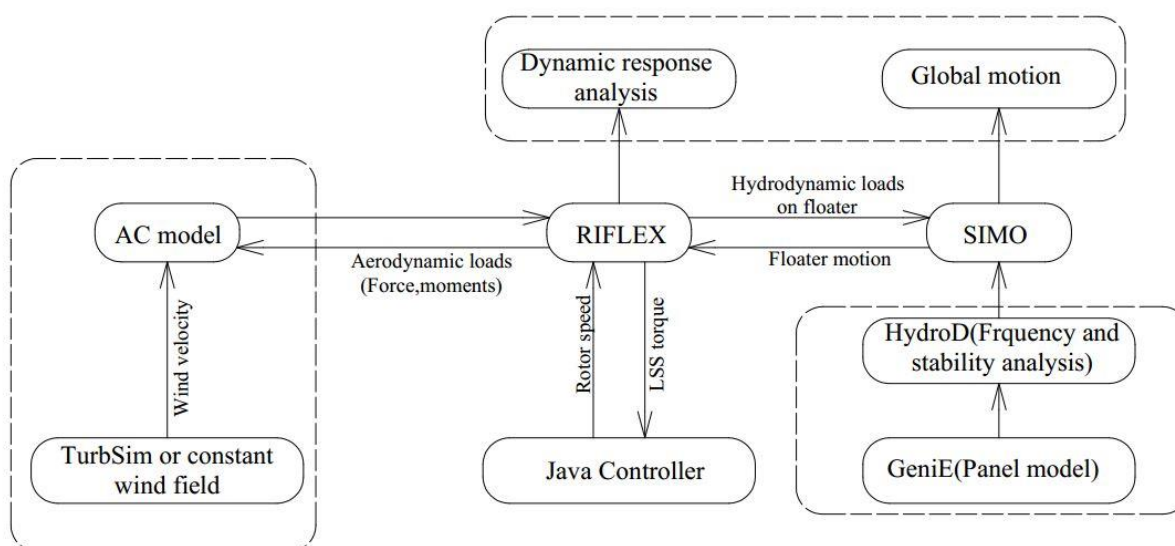
Figure 3.4: Working process of fully coupled simulation tool [21]

3.6   Control Strategy

A PI generator control, developed by Cheng et. al. (2015), is applied to keep the generator power production approximately constant when the rated wind speed is achieved. The design is based on the original model developed by Merz and Svendsen (2013). The control system is shown in the figure below.
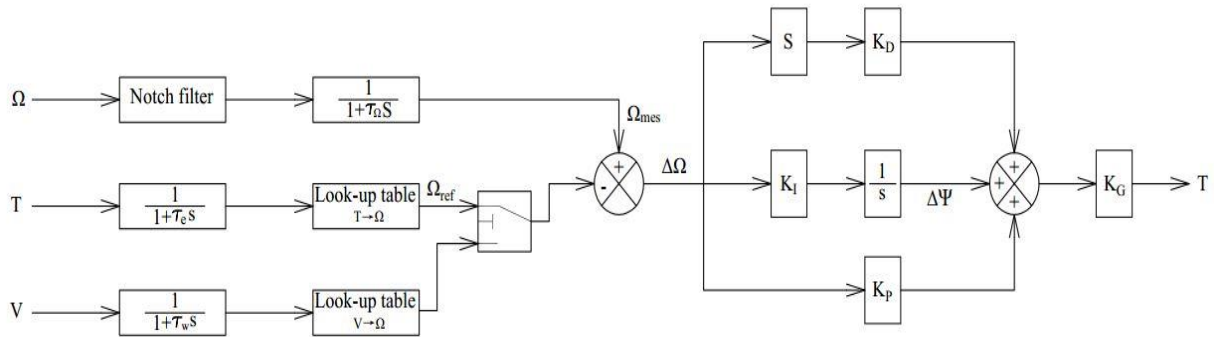
Figure 3.5: The generator control torque for a FVAWT [21]

Electric torque and generator power are measured and low pass filtered. The main aim is to reduce the error between the measured and filtered rotational speed Ω_{mes} and reference rotational speed Ω_{ref}. The reference rotational speed is measured as a function measured wind speed $\hat{V}$ and low-pass filtered electric torque $\hat{T}$. The updated electric torque is given by the following formula when the quantity $\Delta\Omega$ is fed through the proportional, integral and derivative path [21].

$$T(t) = K_G \left(K_P \Delta\Omega(t) + K_I \int_0^t \Delta\Omega(\tau)d\tau + K_D \frac{d}{dt}\Delta\Omega(t) \right) \tag{3.34}$$

In this equation, K_G represents generator stiffness and K_P, K_I and K_D are the proportional, integral and derivative gains respectively [21].

3.7 Load cases and environmental conditions

Several load cases were defined for this study to check the performance FVAWT. These cases are used in the time domain simulation. We applied different wind speed and check the response of the FVAWT. The data are shown in the tabulated form:

Table 3.1: Steady wind load cases for FVAWT

Load cases	$U_w[m/s]$	$H_s[m]$	$T_p[s]$	Wave condition	Simulation length$[m]$
LC1.1	5	---	---	---	3000
LC1.2	8	---	---	---	3000
LC1.3	10	---	---	---	3000
LC1.4	12	---	---	---	3000
LC1.5	14	---	---	---	3000
LC1.6	18	---	---	---	3000
LC1.7	22	---	---	---	3000
LC1.8	25	---	---	---	3000

The potential theory model and the Morrison model then tested with turbulent wind and irregular waves. We have different cases for waves. For each instance, we define different H_s and T_p. The different instances shown in tabular form:

Table 3.2: Load cases for turbulent wind and irregular waves

Load cases	U_w $[m/s]$	H_s $[m]$	T_p $[s]$	T_I $[-]$	Wave condition	Simulation length $[s]$
LC2.1	5	2.10	9.74	0.224	Irregular	4600
LC2.2	8	2.55	9.86	0.174	Irregular	4600
LC2.3	10	2.88	9.98	0.157	Irregular	4600
LC2.4	12	3.24	10.12	0.146	Irregular	4600
LC2.5	14	3.62	10.29	0.138	Irregular	4600
LC2.6	18	4.44	10.66	0.127	Irregular	4600
LC2.7	22	5.32	11.06	0.121	Irregular	4600
LC2.8	25	6.02	11.38	0.117	Irregular	4600

Like steady wind cases, we consider eight different wind speed with rated speed 14 m/s. While for steady wind test H_s is very small but for irregular waves we need to consider this value. The total simulation length was 4600s. But the last 1000s was taken into consideration. This is necessary due to the transient effect on wind turbine.

To generate the turbulent wind, we use TrubSim software. It's been developed to provide numerical simulation of a full field flow that contains turbulent structures and reflect the proper spatiotemporal turbulent velocity relationships[12]. Its purpose is to provide the wind turbine designer with the ability to drive design code simulations. In our study, we use five different seeds for each velocity. In total, we have 40 simulation result that we need to compare with old one as well as measure the fluctuation of turbine output. But for simplicity we only consider one seed for our discussion.

3.7.1   Environment

To design an offshore floating VAWT, we need to consider real environmental situation. First we consider the steady wind condition and then considering wind and wave cases together. In some places, it might necessary to consider the current, ice loads and other loading phenomenon. But for simplicity we neglect this loads from our evaluation.

3.7.2 Wind

In this study, wind field is assumed to be two dimensional, propagating parallel to the horizontal plane. This model includes gust spectra both in the mean direction and normal to the mean direction. The wind profile used for this study is described by:

$$\bar{u}(z) = \overline{u_r}\left(\frac{z}{z_r}\right)^{\alpha} \tag{3.35}$$

where,

z is the height above waterplane

z_r is the reference height

$\overline{u_r}$ is the average velocity at a height z_r above surface

α is the height coefficient (0.10-0.14)

3.7.3 Irregular waves

For simple analysis, we use regular or periodic waves. But this simple model does not give any realistic description for real sea state. So, we use irregular sea wave condition. The description of the sea state is random. We assume that a series of long crested waves. The waves have different amplitudes, frequencies and phase angle. The linear theory is applied to simulate irregular wave. It is considered as a summation of sinusoidal wave components, and the linear long crested wave model is given by [30]:

$$\zeta(t) = \sum_{i=1}^{N} A_i \sin(\omega_i t - k_i x + \mathcal{E}_i) \tag{3.36}$$

where $\zeta(t)$ is the free surface elevation for long crested waves travelling in the x direction, A_i is the wave amplitude, ω_i is the angular frequency, k_i is the wave number and $\mathcal{E}_i$ is the phase angle.

It is usually assumed for long crested waves:

1. The wave process is stationary.
2. The wave elevation is normally distributed with zero mean and variance σ^2.
3. The wave process is ergodic.

Based on the assumption that the wave process follow Gaussian distribution the wave time series is generated by Inverse Fast Fourier Transformation. The Joint Nordic Sea Wave Project(JONSWAP) spectrum has been used for this study.

$$S(\omega) = \frac{\alpha g^2}{\omega^5} \exp\left(-\beta \left(\frac{\omega_p}{\omega}\right)^4\right) \gamma^{exp\left(-\frac{\left(\frac{\omega}{\omega_p}-1\right)^2}{2\sigma^2}\right)} \tag{3.37}$$

$$\alpha = 5.061 \frac{H_s^2}{T_p^4} (1 - 0.287\ln(\gamma)) \tag{3.38}$$

$$\sigma = \begin{cases} 0.07 \; for \; \omega < \omega_p \\ 0.09 \; for \; \omega \geq \omega_p \end{cases} \tag{3.39}$$

In equation 3.37, α is known as spectral parameter and γ is known as peaked parameter which is in our case 3.3.

3.8 Decay test

Considering a mass-spring system, when a body is displaced from its mean position, the body starts oscillating around the mean. But if we consider the damping of the system the amplitude follows an exponential decay. In this study, we applied a force on the platform then release the force. The body starts oscillating in the water. But the damping of water prevents this movement. So, the amplitude decays as the time flows. If we observe the envelop of the amplitude curve, we see the amplitude follows an exponential decay. The solution of the equation is given by the following equation:

$$\eta(t) = e^{\xi \omega_0 t} R \cos(\omega_d t - \theta) \tag{3.40}$$

where, $\omega_d = \omega_0\sqrt{1 - \xi^2}$ and ξ is the damping ratio and ω_0 is the natural frequency. The term, ω_d is known as damping frequency.

For decay test, we applied ramp force and constant amplitude force for a certain amount of time. Then the force was withdrawn and the decay measured. The simulation time varies 1300-1600s for different degrees of freedom. The amplitude of the force also varies for different DOFs. Natural period for six DOF between the new OC4 and the old OC4 model is shown below:

Table 3.3: Natural time period

Degrees of freedom	Time Period for new OC4[s]	Time Period for old OC4[s]
Surge	98.0	113.1460
Sway	97.3	113.1460
Heave	16.2	17.0440
Roll	25.8	20.6790
Pitch	25.4	20.6790
Yaw	72.1	80.4420
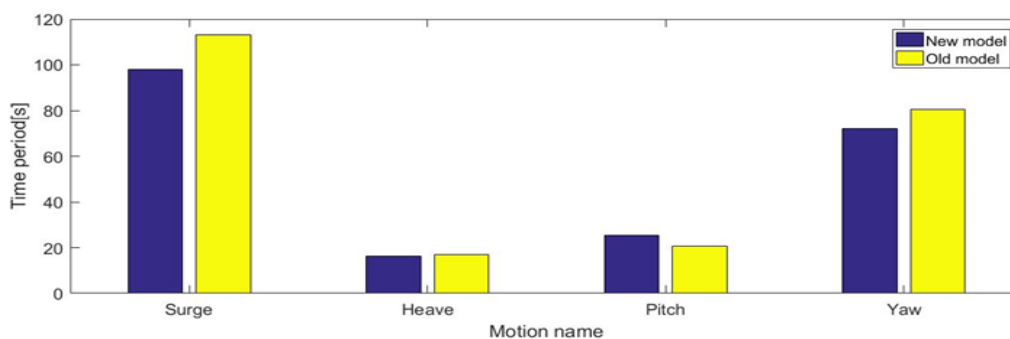
Figure 3.6: Time period for surge, heave, pitch and yaw

3.8.1   Discussion of results (Natural period)

The natural period depends on the mass of the platform, added mass related to the platform and the stiffness of the platform. In the new design, we change several parameters as compared to the old one. They are the dimension of the base column, dimension of the upper column, fairlead position, total mass of the platform and center to center distance of the offset column. The mass was reduced 3500 ton while the diameter of the upper and base column is decreased but the center to center distance increased by two meters. Reducing the diameter of the upper column and base column effectively reduces the water plane area of the platform that in turn reduces the total stiffness of the platform. But increasing the center to center distance increase the stability and stiffness of the platform.

Now as for surge, the fairlead position is changed but the length of the mooring line is same. This reduces the overall stiffness of the mooring line. The mooring line is relatively flexible compared to the old mooring line. In the surge direction, mooring line contributes the stiffness of the platform. As the stiffness reduces so the natural period of surge.

As for heave, they are relatively same with a difference of 0.8s as compared to the old one. The reason behind this decrease in period is that the diameter of the column decreases. This in turn, reduces the stiffness in the vertical direction. Also, mass of the body contributes the overall decrease of the natural heave period.

The same is true for the yaw motion. The natural period of the yaw depends on the water plane area and mass of the body. In the new design, both reduces significantly. This might explain why the natural period of yaw reduces as we compare the old one. But the natural period of pitch increases 4.8s compared to the old one. This might happen due to the increasing distance between two offset columns which increases the stiffness.

3.8.2   Damping ratio and the measurement technique

The ratio of two amplitudes at time step t_i and $t_i + nT_d$ may be found from the measurement and can be found from measurement and used to find the damping of a structure. The ratio can be calculated from the following formula[5]:

$$\frac{u_i}{u_{i+n}} = \frac{u(t_i)}{u(t_i + nT_d)} = \frac{e^{\xi \omega_0 t_i R \cos(\omega_d t_i - \theta)}}{e^{\xi \omega_0 (t_i + nt_d) R \cos(\omega_d(t_i + nt_d) - \theta)}} = e^{-\xi \omega_0 (t_i + nt_d)} \tag{3.41}$$

A measure of damping is to measure the damping for two amplitudes for a certain interval. The logarithmic decrement can be defined as:

$$\wedge = \ln\left[\frac{u_i}{u_{i+1}}\right] \tag{3.42}$$

The connection between $\wedge$ and ξ is expressed by setting n=1 in equation (2.10)

$$\wedge = \xi \omega_0 T_d = 2\pi \frac{\xi}{\sqrt{1-\xi^2}} \approx 2\pi\xi \text{ (As } \xi \text{ is a very small quantity)} \tag{3.43}$$

So, the relation in equation (2.11) gives an approximate formula for damping ratio:

$$\xi \approx \frac{1}{2\pi n} \ln\left[\frac{u_i}{u_{i+n}}\right] \tag{3.44}$$

This is the final that we used for calculating damping ration in our study for six degrees of freedom.

The table and the figures were shown below:

Table 3.4: Damping ratio

Degrees of freedom	Damping ratio for new OC4[s]	Damping ratio for old OC4[s]
Surge	0.04471	0.04216
Sway	0.03738	0.03738
Heave	0.02303	0.02410
Roll	0.02827	0.02827
Pitch	0.02353	0.01718
Yaw	0.01145	0.01603

Figure 3.7: Damping ration for both platform
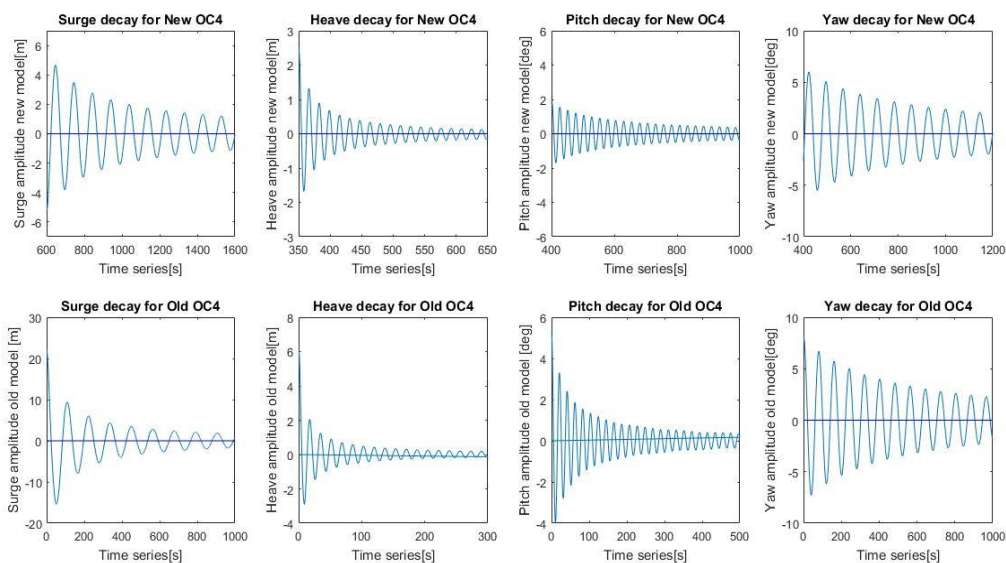
Figure 3.8: Time history of surge, heave, pitch and yaw (decay test)

3.8.3   Discussion of results (Damping ratio)

The damping ration indicates the amount of damping in an oscillation. It's the ration of the damping of a system to the critical damping. Higher value indicates the damping is large and when the value approaches one, there is no oscillation in the medium. The damping ration depends on the mass and the stiffness of a system. If the damping ration is larger, the time period related to the motion is also larger.

In our study, we can see the damping ratio for the old model is relatively larger. This is expected. For the new OC4 semi-submersible we change different parameter such as water plane area, distance, mass and others. As for surge motion, the damping ratio is relatively larger than other motion. So, the time period for surge is also larger than any other case. This happened due to

39

change in stiffness of the mooring line. The mooring lines for the new one is less stiff than the old one.

As for heave, the main contribution came from the base column and the water plane area. As the diameter of the base column reduced this effectively change in damping ratio. For pitch and yaw the damping ratio is larger for the old semi-submersible. This is mainly due to the reduction of water plane area which effectively reduces the stiffness of the platform.

Now if we look at the figure for the decay test two parallel comparison is made for the two semi-submersibles. It shows the time history of decay for different motion when no aerodynamic loads are acting on the system. As we observe, in the beginning of the decay of OC4 semi-submersible the decay was fast. The amplitude decays faster. This is due to the quadratic damping activated at that time. Large amount of water displaced due to rapid movement. So, viscous damping is more important. But as the time increases the amplitude decays slowly. This is due to the activation of first order damping.

3.9   Results and discussions for steady wind test

3.9.1   Global motions

In the steady wind test, different wind loads are acting on the wind turbine. The wave forces are zero by making the significant wave height very small. Then we run the analysis for 3000 s. The first 2000 s is not taken into consideration. Only last 1000 s is considered. Transient effect need to be consider. In order to reach a steady state, we need to wait for the first 2000 s.

At first we want to look at the motion characteristic of the FVAWT against wind speed. Here, the four important degrees of freedom are surge, heave, pitch and yaw. The natural period of surge, heave, pitch and yaw are 98.0s, 16.2s, 25.4s and 72.1s respectively. The tests are carried out in calm water and the turbine is in the parked condition. The wind field is not present and hence aerodynamic forces are not calculated.

Then we applied different steady wind load against VAWT and then noted the mean offset from its original position. The mean offset data is shown below:

Table 3.5: Mean offset under different load cases

Wind speed $[m/s]$	Mean Surge $[m]$	Mean Heave $[m]$	Mean Pitch $[deg]$	Mean Yaw $[deg]$
5	1.2062	-0.0211	0.4874	-0.2758
8	3.1407	-0.0236	1.2309	-0.6845
10	4.9877	-0.0281	1.9349	-1.0498
12	6.6165	-0.0336	2.5325	-1.6566
14	7.9087	-0.0391	2.9948	-2.3945
18	7.2262	-0.0363	2.7144	-2.7659
22	7.6625	-0.0382	2.8738	-2.7888
25	8.2941	-0.0412	3.1039	-2.8533
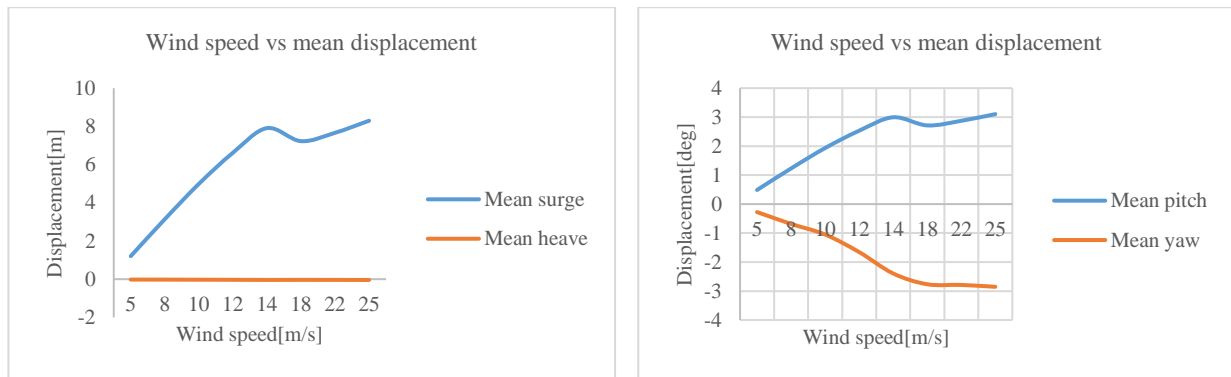
Figure 3.9: Mean offset vs wind speed (surge, heave, pitch and yaw)

As we observed from the figure there is an increasing mean offset pattern in mean surge and pitch motion with a slight deviation around 18 m/s then again follow the increasing pattern. The largest value of surge is 8.2941 m. This is obvious as the stiffness in the surge direction is low compared to heave. Only mooring line contributes the axial force against surge motion. The mean heave is almost zero. The stiffness along the vertical axis is very large which explains why the mean heave is almost zero with a deviation 0.0412 m. The pitch and yaw has a mean offset due to the moment exerted by the constant wind field.

Now we need to compare the value of the current model to the old model. We will consider the mean and standard deviation of the motion such as surge, heave, pitch and yaw.

At first we will take a look at the mean motion of the two model. The mean value of heave and yaw almost identical. But for surge the mean differed with approximately 1 m and for pitch its almost one degree. As we discussed previously, the mooring line is relatively soft in the new model as compared to the old one. So, the displacement is relatively large as we observe in this case.
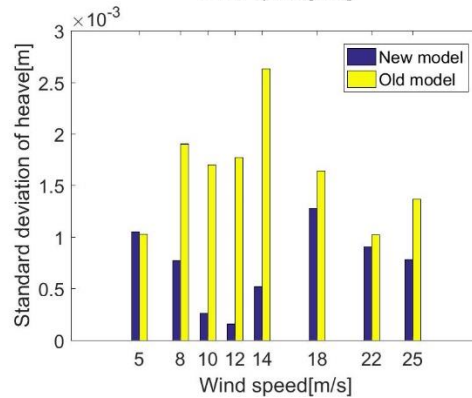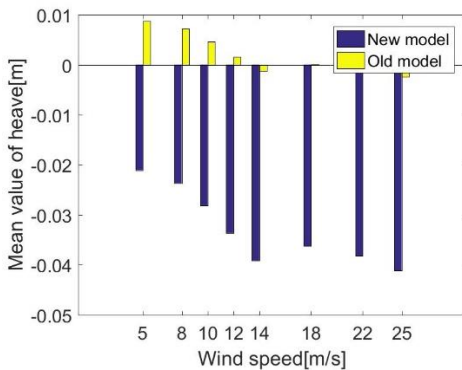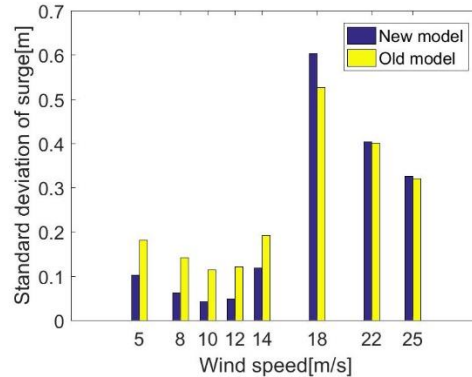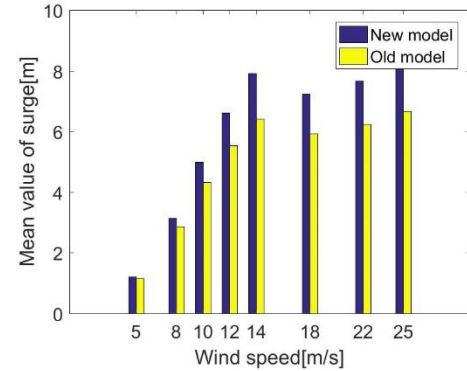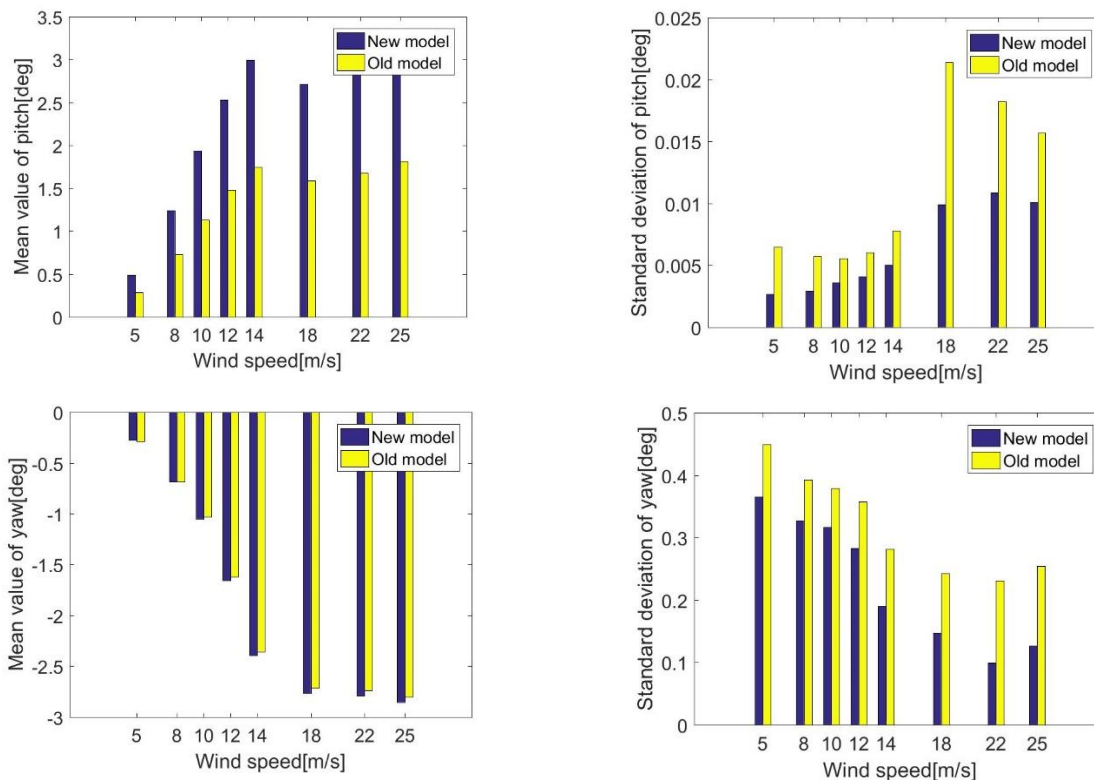
Figure 3.10: Mean offset and standard deviation of motions under different load cases

Now we will compare the standard deviation of the motion. As it is seen from the figure the standard deviation is very small for these four motion. In case of heave and pitch they are very small and for surge this value is 0.1 m and for yaw 0.18 degree approximately. One thing need to be satisfied. In most cases, the first order excitation energy is in the range of 5-15 s. In order to get rid from the resonance our platform natural period must be outside of this range. The only motion that might cause this resonance problem is heave. But if we take the standard deviation of the motion then we realize highest deviation from the mean of a motion component. The deviation of heave is very small.

3.9.2   Turbine performance

Here we include four different parameters for comparison. The parameters are rotor speed, generator power, aerodynamic thrust and aerodynamic torque. In this section, the figure in the left gives the mean and in the right side gives the standard deviation of the parameter. The load cases are equal in each case.
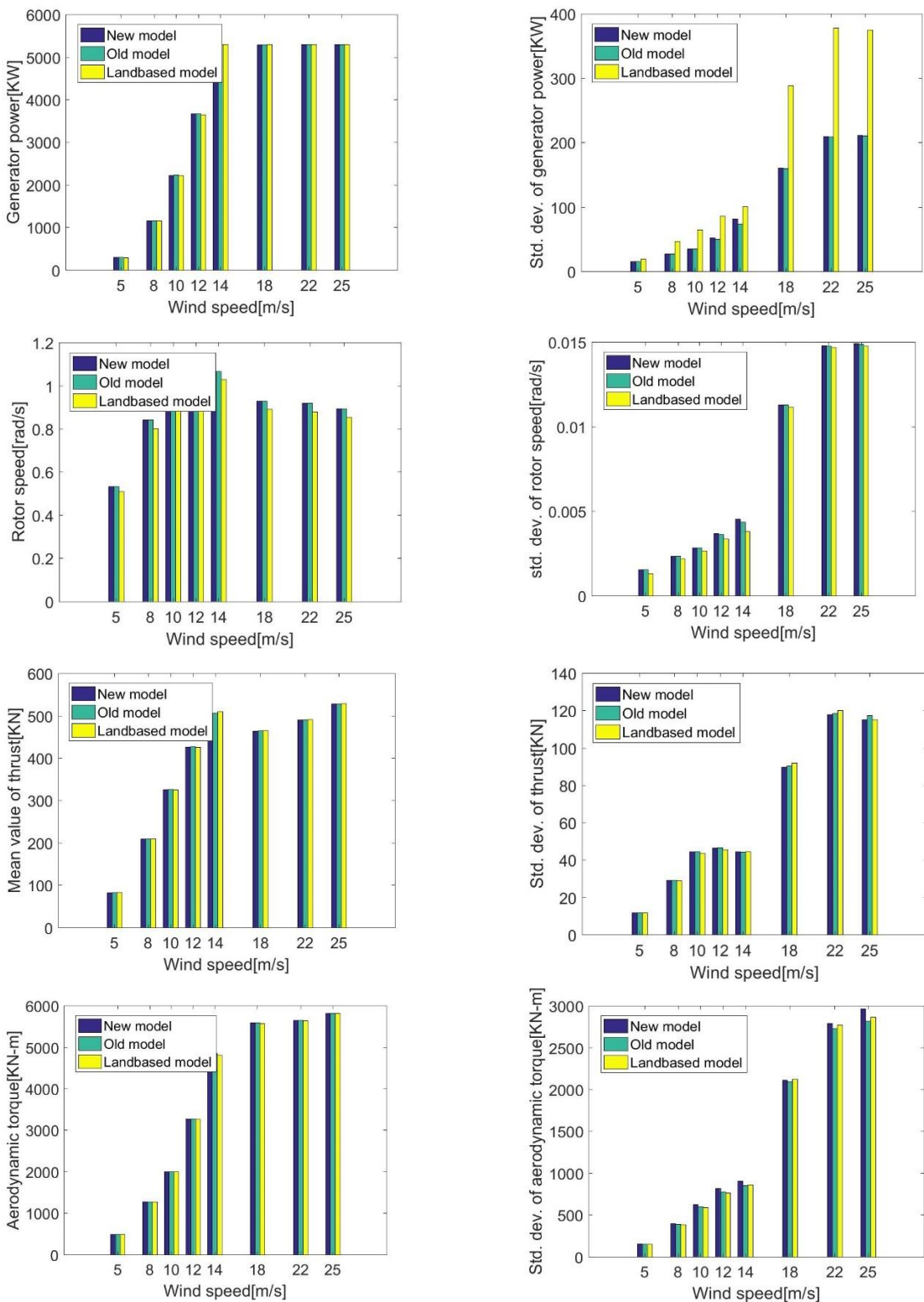
Figure 3.11: Mean and standard deviation of turbine performance (new FVAWT, old FVAWT and landbaed VAWT)

As for the rotor, rotational speed, they show similar performance in each LC. The standard deviation is very small. For generator power the mean value is almost identical in each load cases but there is a large variation of power output for landbased wind turbine than old and new OC4 semi-submersible. Specially the deviation occurs above rated speed. The variation power output occurs in the range of 130-180 KW (above rated speed). Also, if we look at the output of the power we see that above rated speed the output is almost identical but below rated speed, for each load power output increases rapidly.

As for mean thrust they are similar for mean value and standard deviation. The performance is almost similar for thrust. There are two kinds of torque compared here that is generator torque and aerodynamic torque. As for the aerodynamic parameter, they are varying widely and for the generator output they values are relatively small in variation. The aerodynamic variation gives rise to fatigue which leads to failure of different components in the long run. The mean value for both torque is identical. But one significant variation is observed for the standard deviation of generator torque.

3.9.3   Bending moment

A significant study to observe the structural response of the wind turbine. In this case, we choose tower base bending moment. The tower base bending moment is usually caused by the aerodynamic forces and the self-weight of the rotor due to the global roll, pitch and yaw motion of the platform.
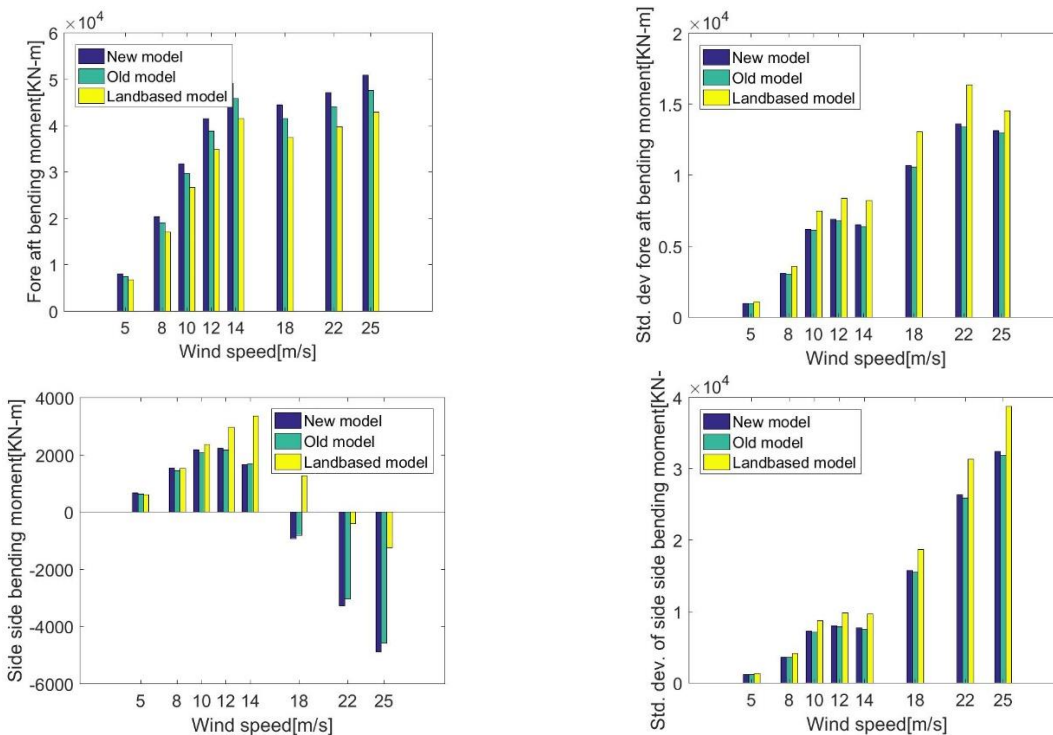
Figure 3.12: Tower base bending moment of wind turbine. Showing mean value and standard deviation for fore-aft and side-side bending moment

When the wind started to flow from the front side of rotor then this side is known as fore side and the opposite part is known as aft side. As wind flows from the front side of the rotor it creates a large bending moment at the tower base which is known as tower base fore-aft bending moment. Remaining side bending moment is known as side-side bending moment. It is obvious that the fore aft bending moment is much larger than the side-side bending moment. It is also evident from the figure of the fore-aft and side-side bending moment.

As for the fore-aft bending moment the largest value found from the new OC4 semi-submersible. This can be explained in following way. The weight of the new OC4 semi-submersible is greatly reduced. This increases the angular motion of the new semi-submersible because same load is acting on the lighter platform. This increases the angular offset of the new platform compared to the old platform. Extra increment of the angular offset compensated by the large fore-aft bending moment. But for bottom fixed turbine there is no such motion. The standard deviation is very large for the fore-aft bending moment. This might lead to fatigue of different component in the long run. Standard deviation is always larger for landbased wind turbine.

As for side-side bending moment the largest bending moment found from landbased wind turbine. Also, above rated speed the bending moment acting in the opposite direction. The standard deviation is also large for side-side bending moment.

3.9.4   Mooring line tension

In this analysis, the mooring line is divided into two parts. One part is connected to the platform and the other rest on the sea bed. Here we are comparing the first part. Tension which is acted on the three-catenary mooring line is compared to the old model.

The axial force acting on the mooring line is almost similar for all load cases. But there is a difference in the standard deviation of axial force acting on the mooring line. It's obvious from the above figure that the standard deviation for the older one is larger than the new one. The largest force acting on the mooring line 2. This is expected as the BC-2 column is directed towards the wave and wind direction. Also, the force in the mooring line 1 and 2 have same magnitude. This happens due to the symmetry of the platform: So, the total forces distributed in the two mooring lines.
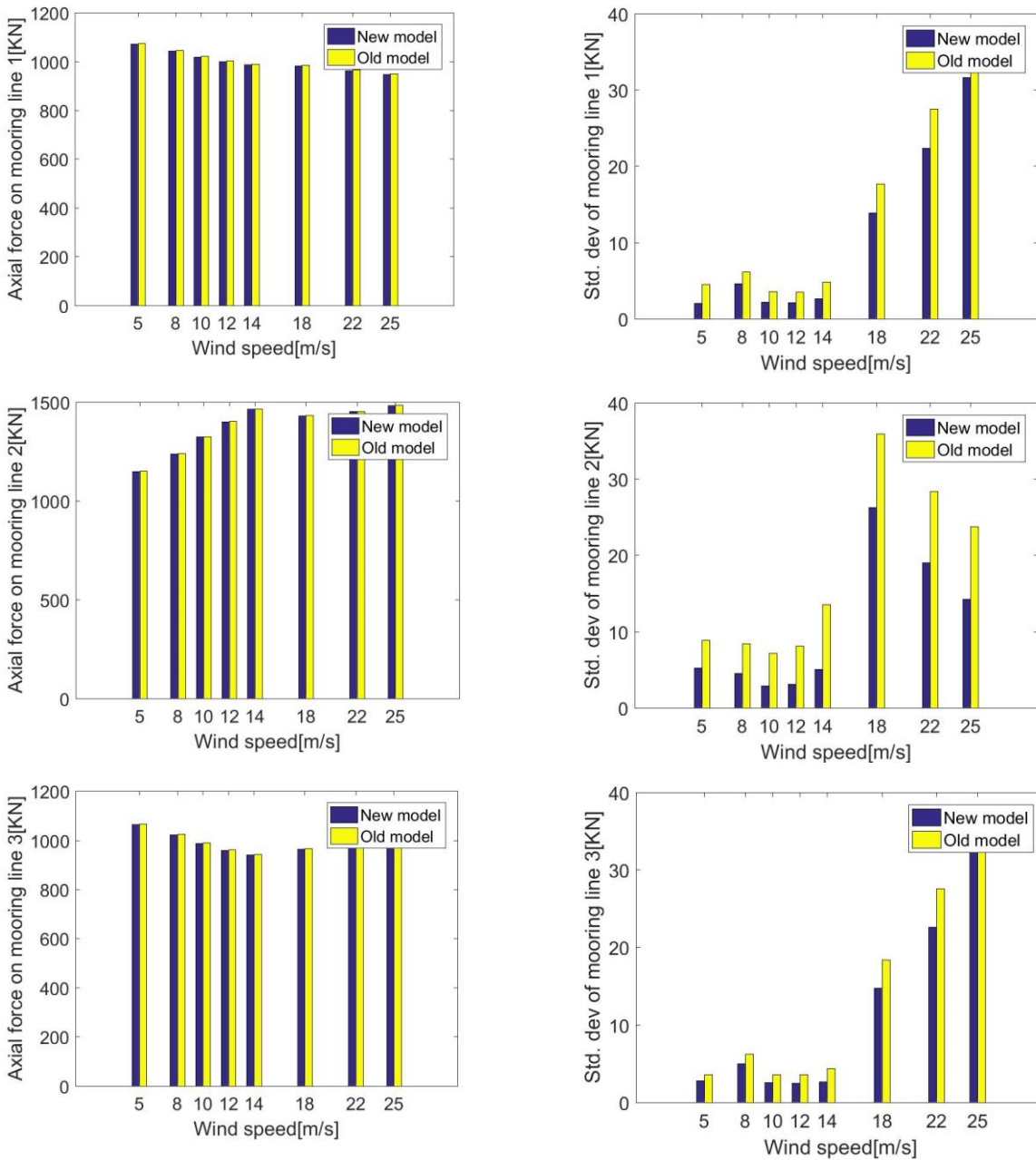
Figure 3.13: Mean and standard deviation of axial force on mooring line 1, 2 and 3

3.10 Turbulent wind and irregular waves (Results and discussion)

3.10.1 Global motion

For Darrieus FVAWTs, the mean deviation of platform motion was mainly due to the load exerted by the wind field. This concept is applicable for straight bladed floating VAWT which is considered in this study. Here we present the data comparison for seed 1. The highest mean value of surge occurs at 25 m/s and the maximum value is 8 m. The mean value of pitch and yaw is 3.15 degrees and -2.87 degrees respectively. As for sway, heave and roll the deflection from its mean value is small. As for this motion the stiffness and damping in the respective direction is very large. As for surge, pitch and yaw the mean value of motion is increasing and the highest at 14 m/s and the increasing rate is approximately constant or very small. Also, the deflection from the mean value is larger than the previous OC4 model. The effect of mean value of motion for different load cases is shown the following figure 3.14.
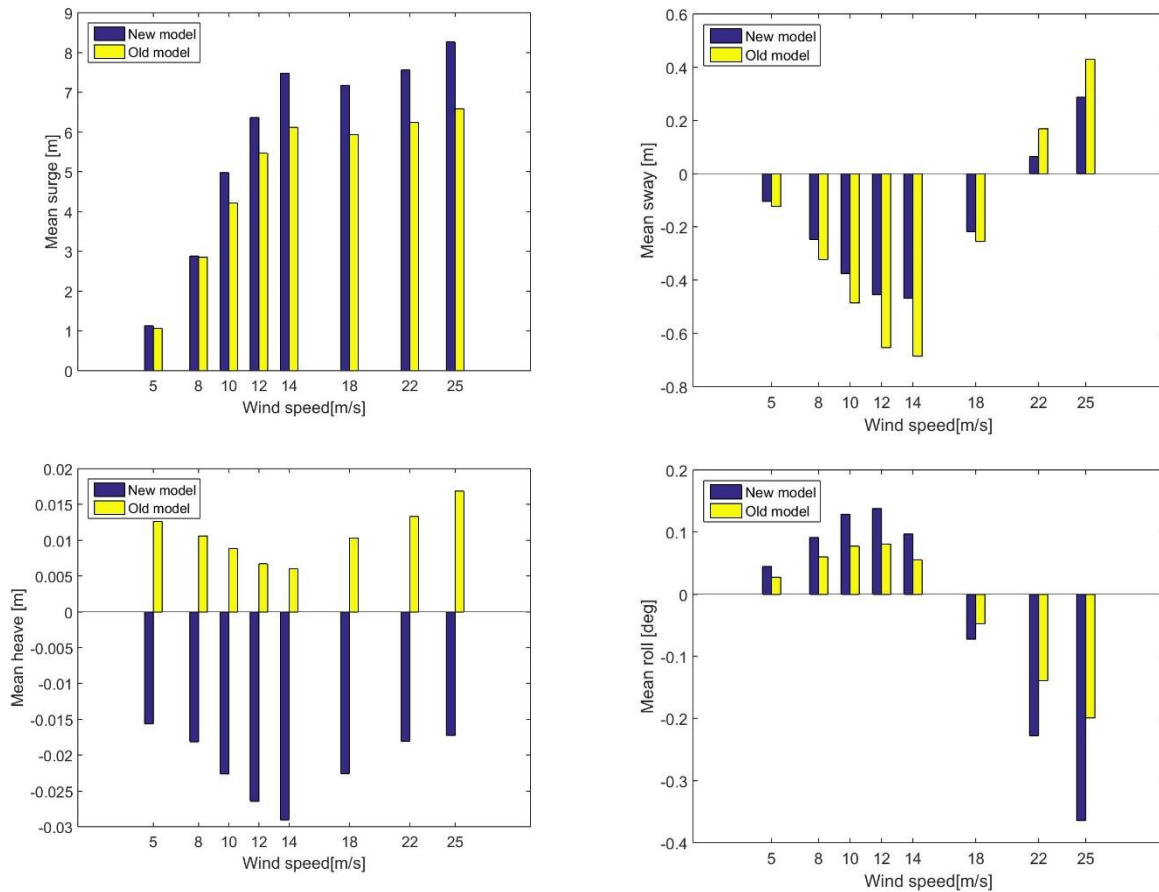
Figure 3.14(a): Mean offset of of different degrees of freedom
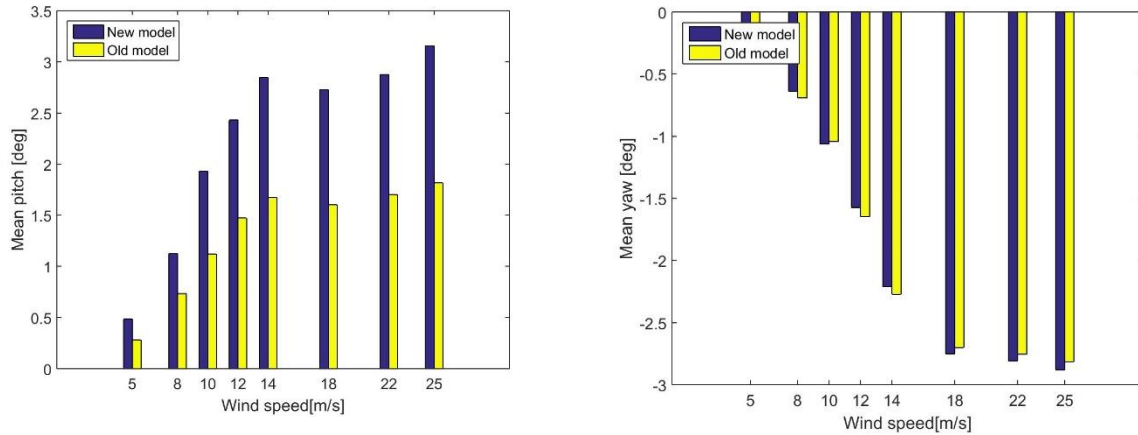
Figure 3.14(b): Mean offset of of different degrees of freedom

The standard deviation is highest for surge and yaw. As for surge motion highest deviation occurred for surge at 12 m/s and the value of deviation is 1.733 m for new model and for old model the maximum deviation occurs at 10 ms^{-1} wind velocity. As for yaw motion the maximum deviation occurs for new and old model at rated speed and the deviation is 1.374 and 1.092 degrees respectively. For other motions, the mean value is small so the standard deviation is also small. The discrepency in between two platform is mainly due to the changing of different design parameters.
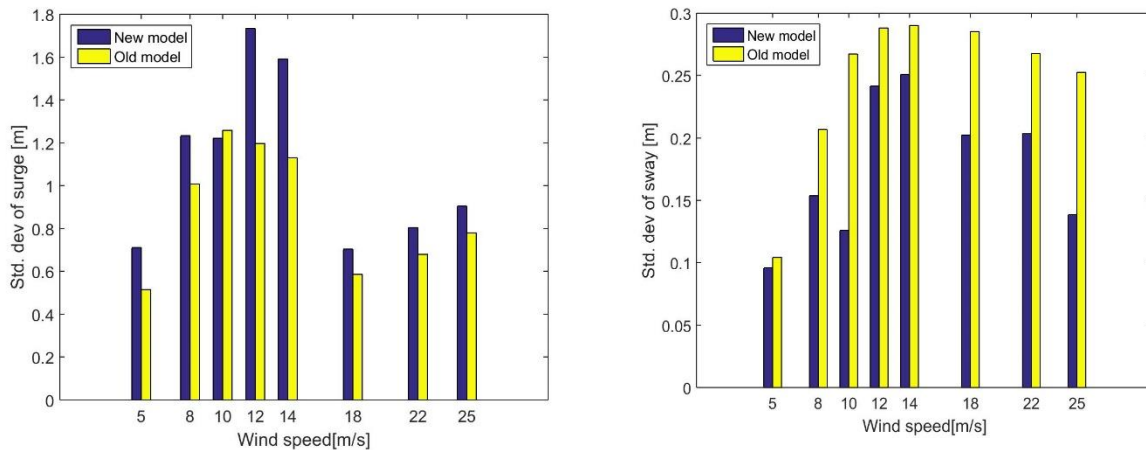
Figure 3.15(a): Standard deviation of surge, sway
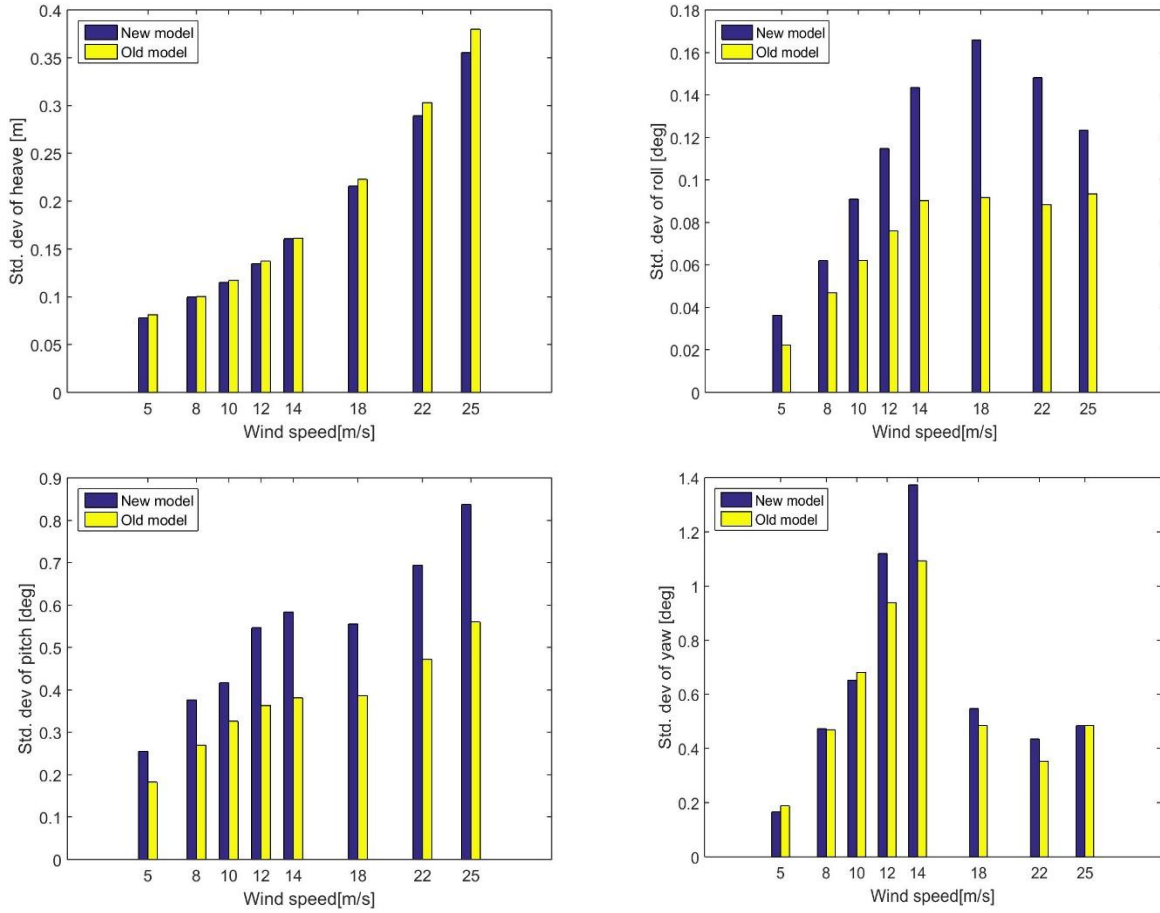
Figure 3.15(b): Standard deviation of heave, roll, pitch and yaw

Power spectral analysis is carried out for surge and yaw for load cases LC 1.3 and LC 1.7. The main contribution of surge and yaw coming from the wind velocity. The figure is shown below:
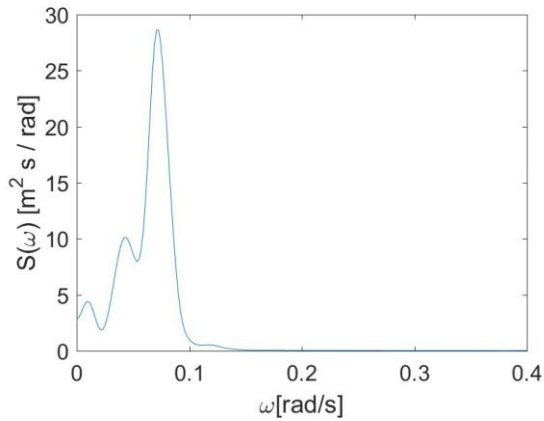
Figure 3.16(a): Power spectra for surge at LC 2.3
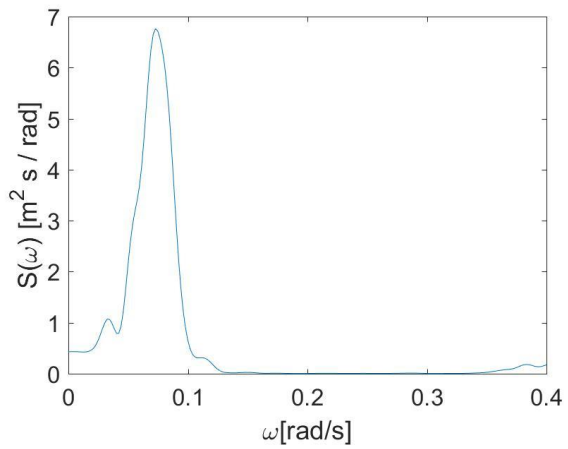
Figure 3.13(b): Power spectra for surge at LC 2.7
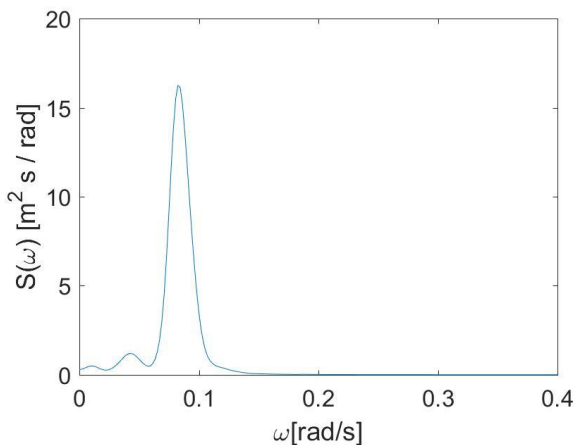
Figure 3.16(c): Power spectra for yaw at LC 2.3
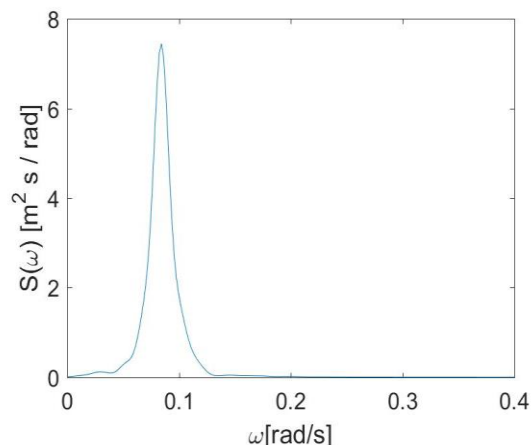
Figure 3.16(d): Power spectra for yaw at LC 2.7

The main contribution came from the wind velocity as shown by the large peak. The smaller peak came from the wave contribution but there is another peak for surge at LC1.7. The main contribution lies in 0.07-0.08 rad/s.

3.10.2   Turbine performance

In our study, we are interested to look at the performance parameters such as rotor speed, power, thrust and torque. As for generator power above rated speed the power production is almost similar for both model. The maximum power produced for the wind turbine occurs at 14 m/s and the power available in the generator is 5.2 MW approximately for both model. As for rotor speed the maximum speed found at 14 m/s and then speed decreases gradually. The mean value of thrust and torque follows the same pattern. Above rated speed the value increases slowly compared to the value below rated speed. The mean value of maximum thrust occurs at 25 m/s and the value is 533 KN. For both model the value of the parameters are very close.
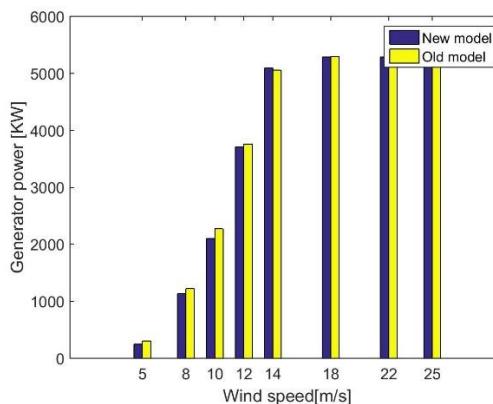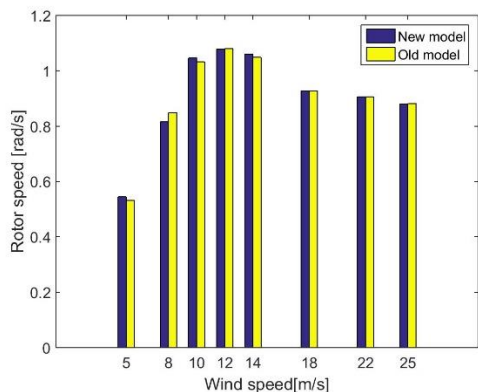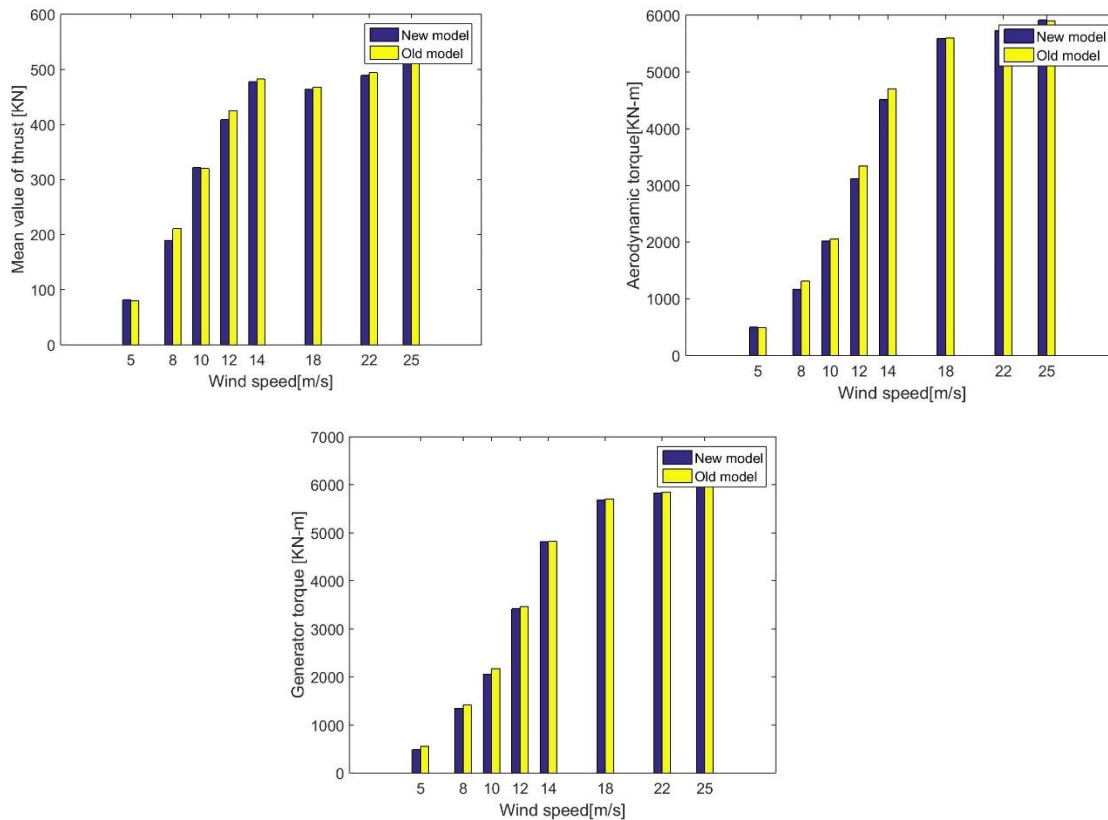
Figure 3.17: Mean value of rotor speed, generator power, thrust and torque

As for rotor speed, the standard deviation is relatively small for both cases. As power in the generator, the maximum deviation occurs at 14 m/s and the rated generator power is 1006.4 KW. It's a very large deviation from the mean value. This is expected due to the huge fluctuation occur for vertical axis wind turbine. It increases the possibility to reduce the life span of different component of wind turbine as it leads to the fatigue of the structure. As for thrust and torque the result differs slightly.
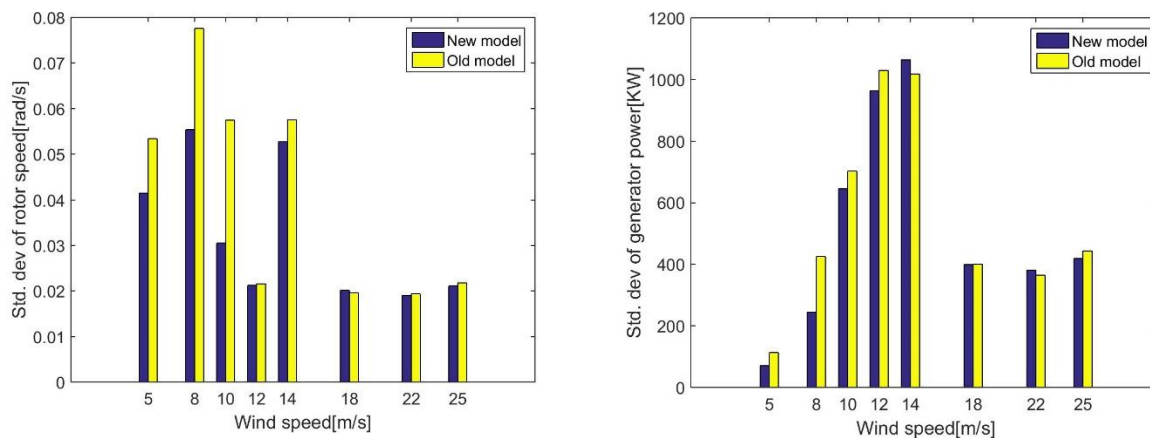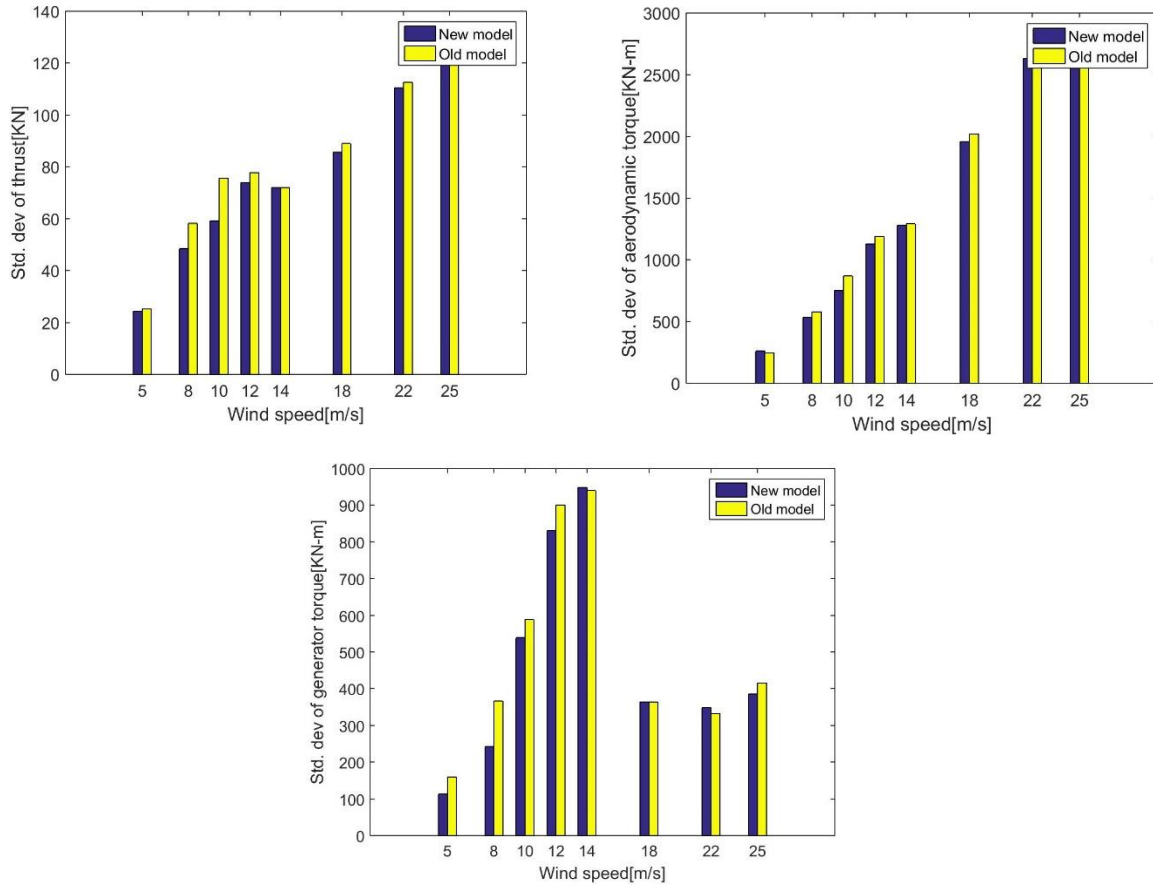
Figure 3.18: Standard deviation of turbine performance

3.10.3 Mooring line tension

To secure the OC4 platform we need to moored the platform with three catenary mooring lines spreading symmetrically through vertical axis [25]. The fairleads are located at the top of the base column which 14 m below the sea water line. Mooring line is divided into two parts. One is mooring part which is connected to the platform and the other one is anchor which rest on the seabed. Each line is separated from the other by 120 degree. One line is directed to the positive x axis and the other two lines are symmetrically distributed with respect to the x axis. Each line has an unstretched length 835.5 m and an equivalent mass per unit length 113.35 kg/m [25].

Here we used linearized mooring model. It should be noted that the mooring arrangement in old platform is opposite than the new model. The result is shown below:
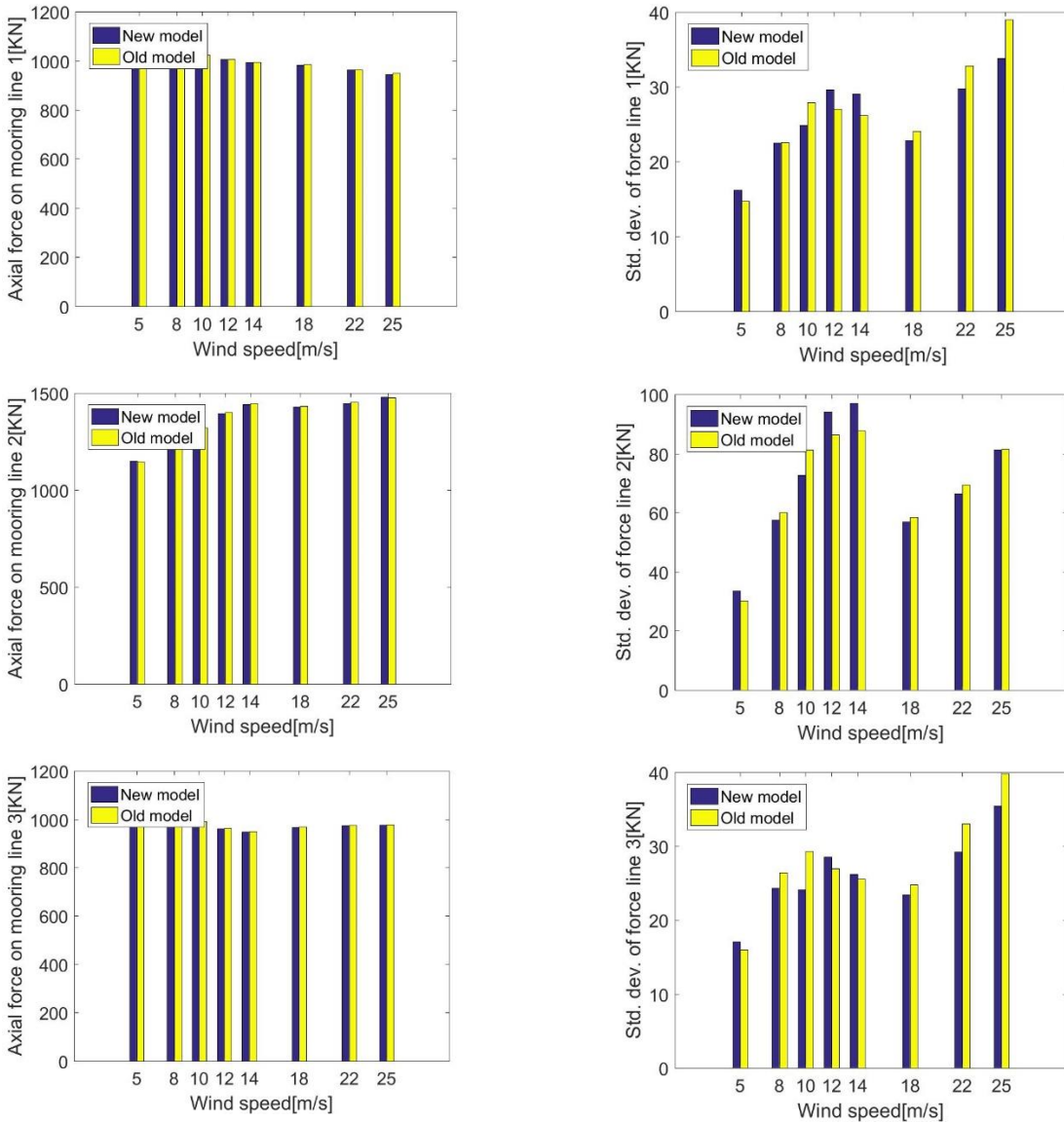
Figure 3.19: Tension on mooring line 1, 2 and 3

The forces in the mooring line is almost similar but there exists deviation in the mooring line force. The largest force acting on the mooring line 2 due to its heading in the opposite direction of the wave and wind. So, the standard deviation is also large for the mooring line 2. As for the 1st and the 3rd mooring line, the force acting on them are of the same magnitude. This is possible due to the symmetry of the platform. So, when the wind and wave hits on the platform the forces are distributed on both lines.

Power spectral analysis was carried out to understand the contribution from different forces. In our cases, only two loads are acting here. They are wind loads and wave loads. The analysis is carried out for wind speed 10 and 22 ms^{-1}. The mooring line we consider here for power spectral analysis is the mooring line 2. The figure is shown below:
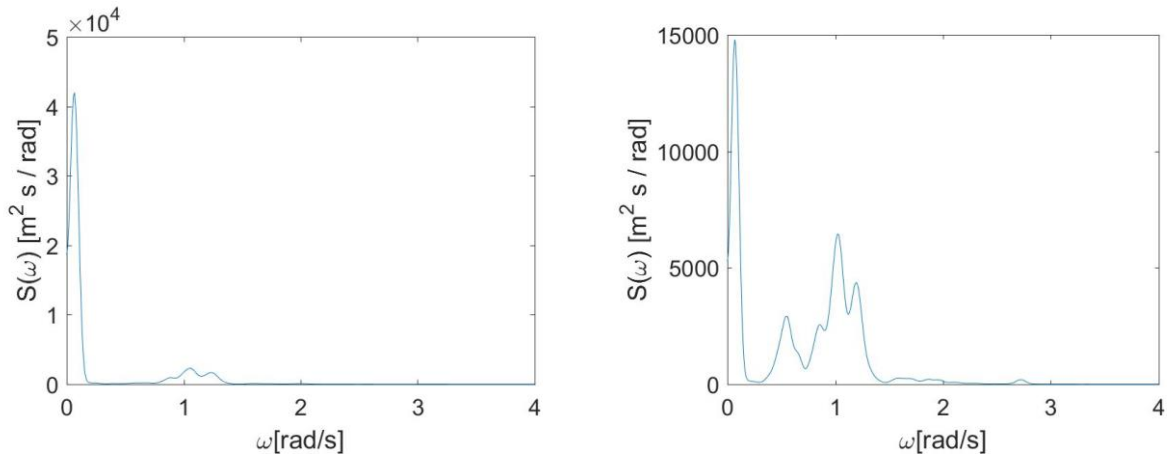
Figure 3.20: Power spectra for mooring line 2 at LC 2.3 and LC 2.7

The main contribution came from the wind. But there are contributions that came from waves. As for LC 2.7 the contribution came from the waves. At 1 rad/s there are some peak which is wave effects on the mooring line.

3.10.4   Bending moment

In our study, we are also interested to study the effect of tower base bending moment. The bending moment in the tower base mainly caused due to the wind loads acting on the rotor as well as by the self-weight of the platforms pitch and roll motions.

The tower base bending moment for the new one is larger than the old OC4 model. This is due to the pitch motion of the new one increases. The moment acting in y direction is known as fore aft bending moment and the one acting in the z direction is known as side-side bending moment. The fore aft bending moment is much higher than the older one. Above rated speed the fore aft bending moment increases slowly than fore aft bending moment below rated speed. But the side-side bending moment takes negative value above rated wind speed. But the standard deviation is large for both cases which might reduce the fatigue life of the platform. This happen due to the varying force acting on wind turbine.
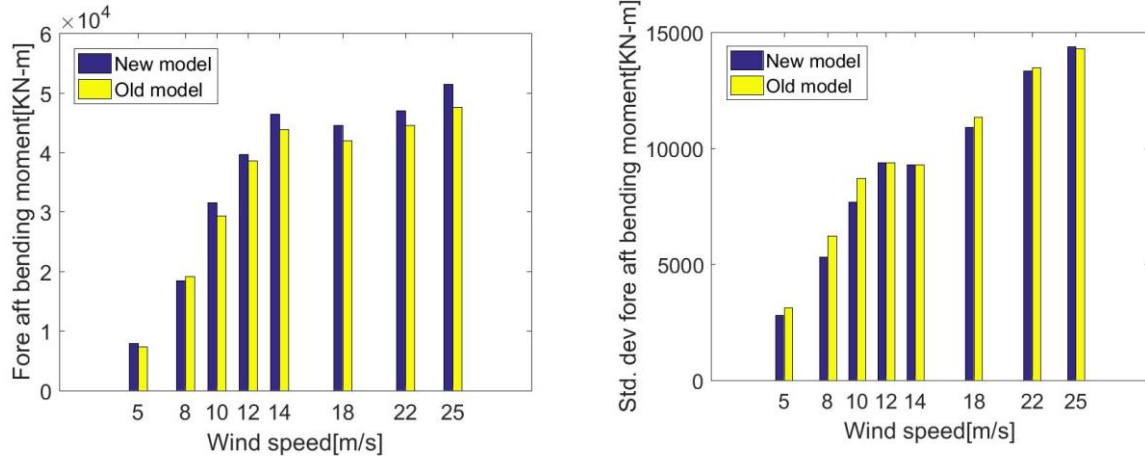
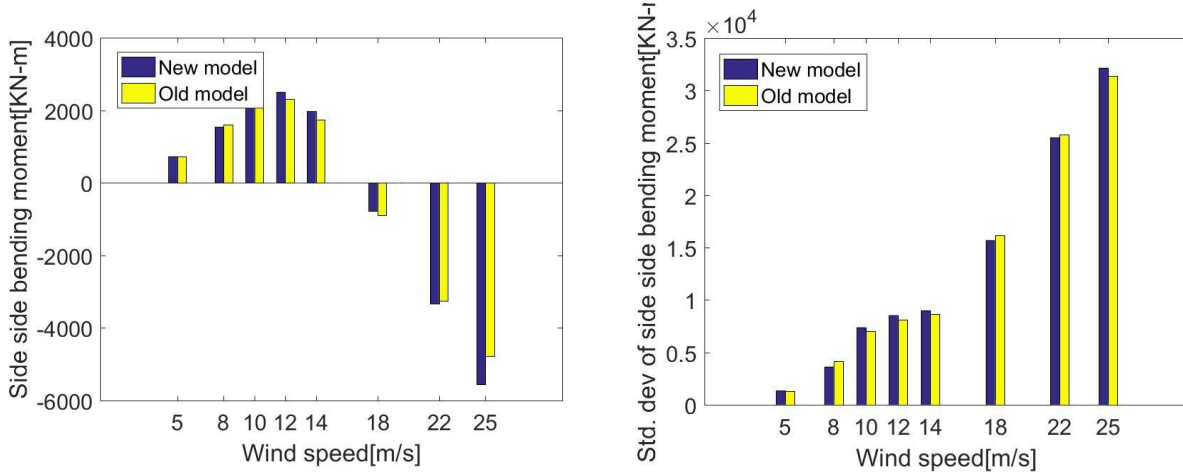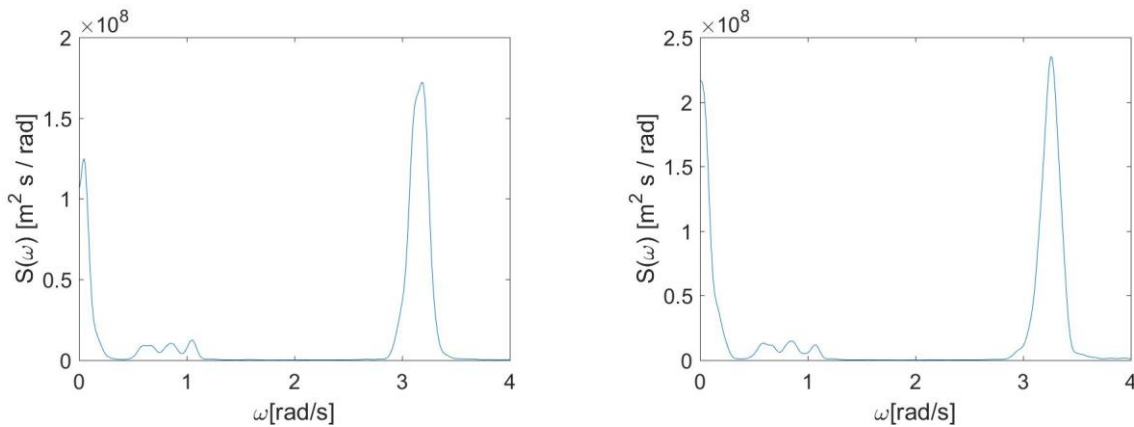*Figure 3.21: Tower base fore-aft bending moment*

Figure 3.22: Tower base side-side bending moment

The spectral analysis is necessary to understand the contribution of different loads. As it is a three bladed VAWT, 3P responses are prominent. The figure is shown below:
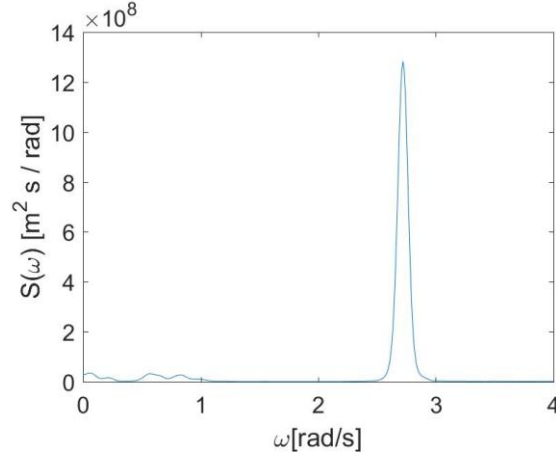
Figure 3.23: Tower base fore-aft bending moment for LC 2.3, LC 2.5 and LC 2.7

In between 0.3-1.2 rad/s, the response came from the wave response but the main contribution came from the wind. Increasing the load, rises the peak significantly as it is evident from the figure.

3.11   Second order effect

So far we have discussed in this study based on the first order property of the wave. Now we want to study the effect of second order on the performance of the new OC4 semi-submersible. Second order effects cause on the loads or motions. There are three effects. They are as follows.

- A mean value force (drift force)
- A sum wave frequency oscillatory behavior ($\omega_i - \omega_j$)
- A difference frequency oscillatory behavior ($\omega_i + \omega_j$)

For a sea state with S(ω), ω_i, ω_j are the two regular wave components. Suppose two incident wave components of a sea state with spectrum S(ω) and two waves with amplitude ζ_{a1} and ζ_{a2} and frequency ω_1 and ω_2. The velocity potential is given by [31]

$$\phi_{01}^{(1)} = \frac{g\zeta_{a1}}{\omega_1} e^{k_1 z} \cos(\omega_1 t - k_1 x + \alpha_1) \quad \phi_{02}^{(2)} = \frac{g\zeta_{a2}}{\omega_2} e^{k_2 z} \cos(\omega_2 t - k_2 x + \alpha_2) \quad (3.45)$$

Velocity potential, is given by the following equation:

$$\phi = \phi_1 + \phi_2 = \phi_1^{(1)}(\omega_1) + \phi_1^{(2)}(\omega_2) + \phi_2(\omega_1, \omega_2) \quad (3.46)$$

Here $\phi_2(\omega_1, \omega_2)$ is the combined effect of the incident waves. We analyze the features of the loads associated with the contribution $(\frac{\partial \phi_1}{\partial x})^2$ to the square velocity term at x=0.

$$\frac{\partial \phi_1}{\partial x} = A_1 \cos(\omega_1 t + \varepsilon_1) + A_2 \cos(\omega_2 t + \varepsilon_2)$$

$$\left(\frac{\partial \phi_1}{\partial x}\right)^2 = A_1{}^2 \cos^2(\omega_1 t + \varepsilon_1) + A_2{}^2 \cos^2(\omega_2 t + \varepsilon_2) + 2A_1 A_2(\omega_1 t + \varepsilon_1)(\omega_2 t + \varepsilon_2) \quad (3.47)$$

$$\left(\frac{\partial\phi_1}{\partial x}\right)^2 = \frac{A_1{}^2 + A_2{}^2}{2} + A_1{}^2 \cos\frac{[2(\omega_1 t + \varepsilon_1)]}{2}$$
$$+ A_2{}^2 \cos\frac{[2(\omega_2 t + \varepsilon_2)]}{2} + A_1 A_2 \cos(\omega_1 + \omega_2)t + \varepsilon_1 + \varepsilon_2$$
$$+ A_1 A_2 \cos(\omega_1 - \omega_2)t + \varepsilon_1 - \varepsilon_2$$

So, the first term in the equation is a constant term which we are going to deal with. This is the known as mean drift force [31].

3.12   Modelling in HydroD

First, the platform is modelled as a 3D panel model is GeniE. We define the mesh size in GeniE 1.2 m. Then export the FEM model in HydroD. Then we use frequency domain analysis to find out the response of the body. We use second order drift force in our calculation. The wave heading angle is selected from 0°-180° with an interval of 30°. Sixty frequency was chosen for the analysis and total depth is 200 m. The SESAM interface file is then import in the SIMO to create a system description file. The final model is then modified according to the description in chapter 2. They are buoyancy compensation factor, design of slender element etc.

There are different technique available for estimating the drift force. Some of them are the direct pressure integration and conservation of the fluid momentum. In our study, we use pressure integration technique in which integration is carried out along the instantaneous wetted surface area of the body [31].

$$F = \int p\boldsymbol{n}ds = -\rho \int_{S_B} \left(\frac{\partial\phi}{\partial t} + \frac{1}{2}|\nabla\phi|^2 + gz\right)\boldsymbol{n}ds = 0 \tag{3.48}$$

3.13   Newman approximation

Consider a sea state with wave spectrum $S(\omega)$. Then the amplitude is given by

$$A_j = \sqrt{2S(\omega_j)\Delta\omega} \tag{3.49}$$

Now we extend the two waves expressing the second-order loads due to the sea state as

$$F_i^{SV} = \sum_{j=1}^{N}\sum_{k=1}^{N} A_j A_k \left[T_{jk}^{ic}\cos(\omega_k - \omega_j)t + (\varepsilon_k - \varepsilon_j) + T_{jk}^{is}\sin(\omega_k - \omega_j)t + (\varepsilon_k - \varepsilon_j)\right] \tag{3.50}$$

This equation includes both the mean and slow drift contributions. The second order transfer functions in the equation is difficult to compute and very time consuming. Newman approximated the equation in the following way. According to Newman we can simplify the equation with the following assumption [31]:

$$T_{jk}^{ic} = T_{kj}^{ic} = \frac{1}{2}(T_{jj}^{ic} + T_{kk}^{ic}) \text{ and } T_{jk}^{is} = -T_{kj}^{is} \tag{3.51}$$

It implies that the values of the second order transfer functions along the line $\omega_j = \omega_k$. If we observe the equation it satisfies when j=k. The approximation holds good if:

- The second order transfer function is close to the line $\omega_j = \omega_k$.
- T_{jk}^{ic} and T_{kj}^{ic} do not change much with the frequency.

If both conditions hold true, then $T_{jj}^{ic} \cong T_{kk}^{ic}$ and we have [31]

$$0.5(T_{jj}^{ic} + T_{kk}^{ic}) \cong \sqrt{T_{jj}^{ic} T_{kk}^{ic}} \tag{3.52}$$

This means we can use geometric mean to approximate T_{jk}^{ic} and T_{kj}^{ic}. Introducing Newman approximation along with geometric mean in the main expression gives:

$$F_i^{SV} \cong \sum_{j=1}^{N} \sum_{k=1}^{N} A_j A_k \sqrt{T_{jj}^{ic} T_{kk}^{ic}} \cos(\omega_k - \omega_j)t + (\varepsilon_k - \varepsilon_j) \tag{3.53}$$

The resulting solution depends only on the transfer function T_{jj}^{ic} and T_{kk}^{ic}. They depend only on the first order linear solution if there is no current and forward motion. So, per the Newman approximation it's no longer necessary to calculate the second order velocity potential ϕ_2. This in turn significantly reduces the labor and the computational cost.

3.14   Results and discussion on the effect of mean drift

Prior to comparative study, A series of load tests was evaluated. Here we use turbulent and irregular wave condition and observe the effect of mean drift force. We used eight different load cases for wind and used seed 1 to generate the turbulent wind by using TurbSim. Then we perform the simulation for 4600s and evaluate the value of last 1000s due to the transient effect of wind turbine and compared the result with the first order effect. Same load cases are used for second order effect as we used for turbulent and irregular waves. The results will be discussed in different section.

3.14.1   Platform motion

Due to the difference in wave interaction in the platform the small variation in the results might be expected. The figure shows the mean and standard deviation of the motion such as surge, heave, pitch and yaw. The trend lines are very similar compared to the first order model. The trends in the mean value of surge, heave are very similar though they differed by their amplitude. The reason is that the mean offset is caused by the wind thrust force. As the stiffness in the heave direction is

larger the deviation is very small compared to surge motion. The sway and roll motions are caused by the aerodynamic lateral loads acting on the rotor. The trend line is also similar in this case. The main contribution of stiffness in the surge and sway direction is coming from the catenary mooring line and for other motions, the water place area contributes the stiffness of the platform.
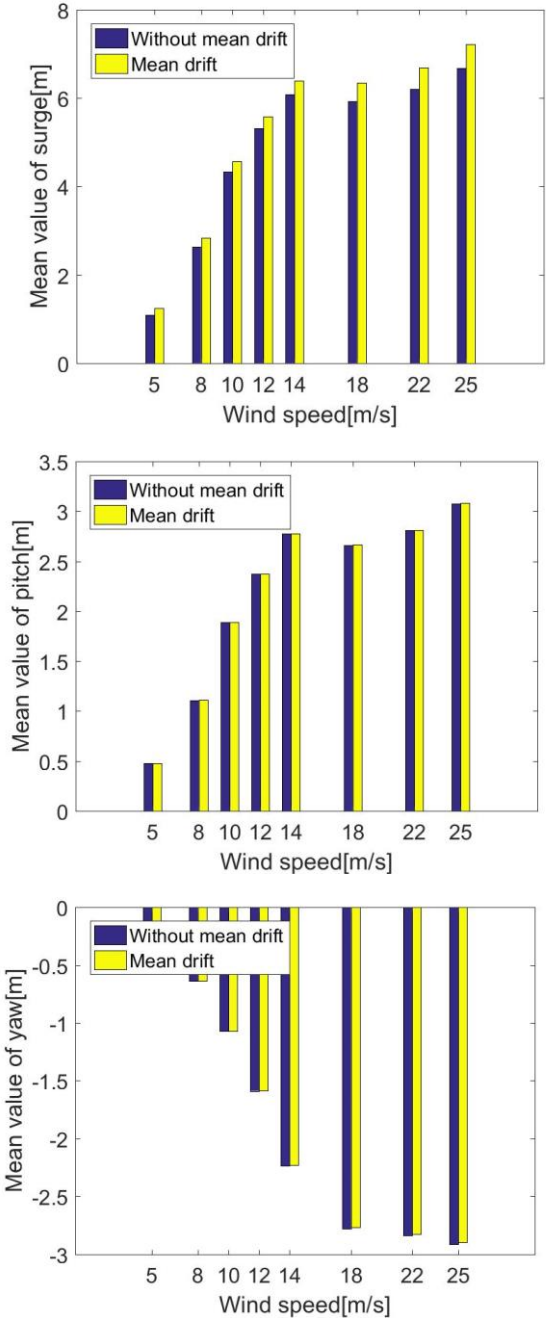

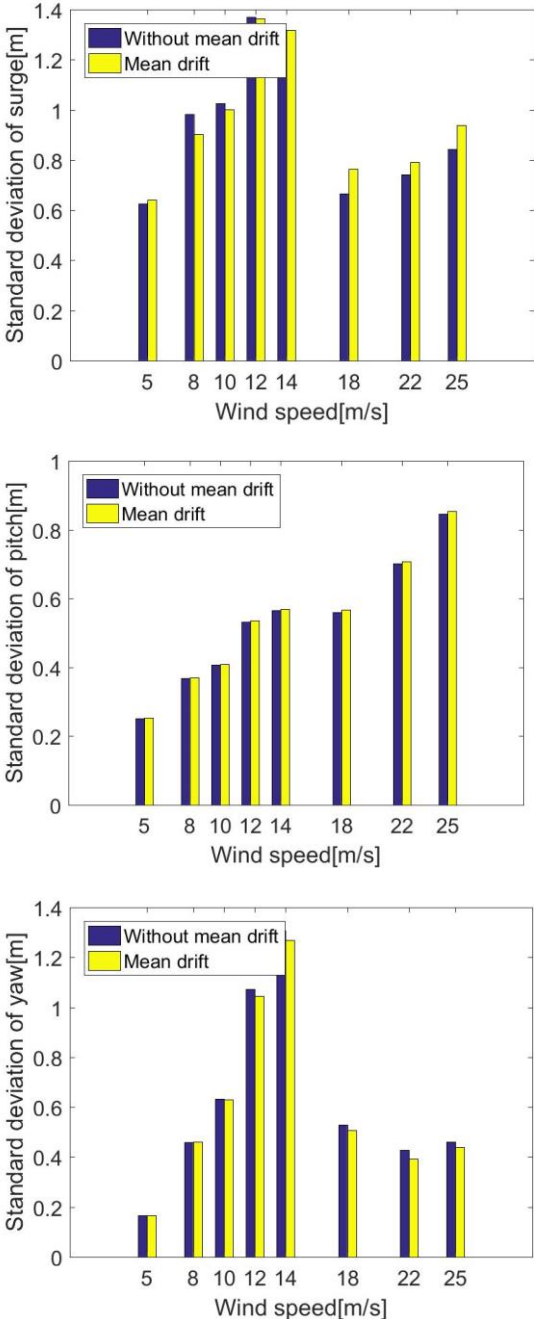*Figure 3.24: Mean offset of surge, pitch and yaw(mean drfit)*

Figure 3.25: Standard deviation of surge, pitch and yaw(mean drfit)

Power spectral analysis will reveal the contributions from different loads. The surge and yaw are considered here. Here, we consider load cases LC 2.3 and LC 2.7.
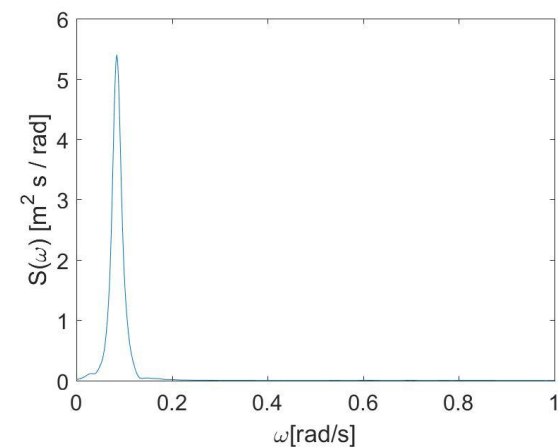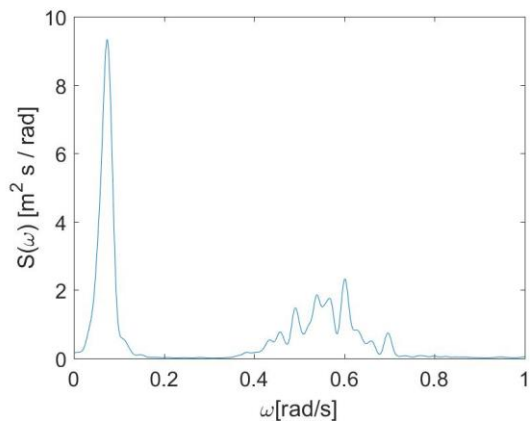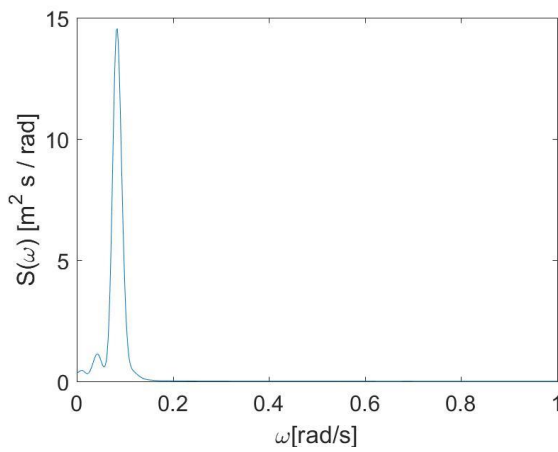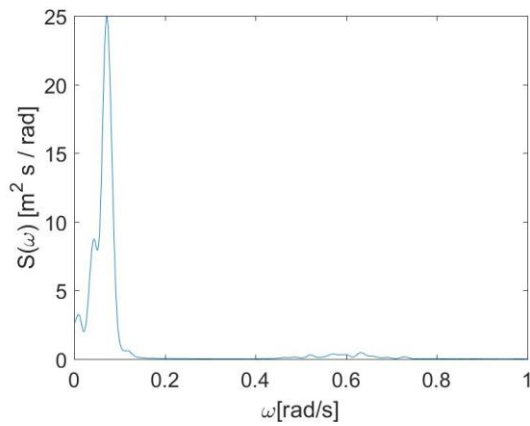

Figure 3.26: Power spectrum analysis for surge under LC 2.3 and LC 2.7

Figure 3.27: Power spectrum analysis for surge under LC 2.3 and LC 2.7

The main contribution came from the wind for both cases. But from 0.4-0.8 rad/s there are some contributions came from waves. At increasing loads the waves loads are significant for surge. But for other cases, it is not so important.

3.14.2   Performance

Here we include thrust, generator power torque of the wind turbine. The rated speed for both cases is 14 ms^{-1}. Above rated wind speed the mean power of the generator is constant because we employ an improved control strategy. Below rated wind speed the power out is steeper. The highest rated output is approximately 5 MW. There is a slight drop in generator at rated speed for mean drift case. But the standard deviation is increases from 8-12 ms^{-1}.
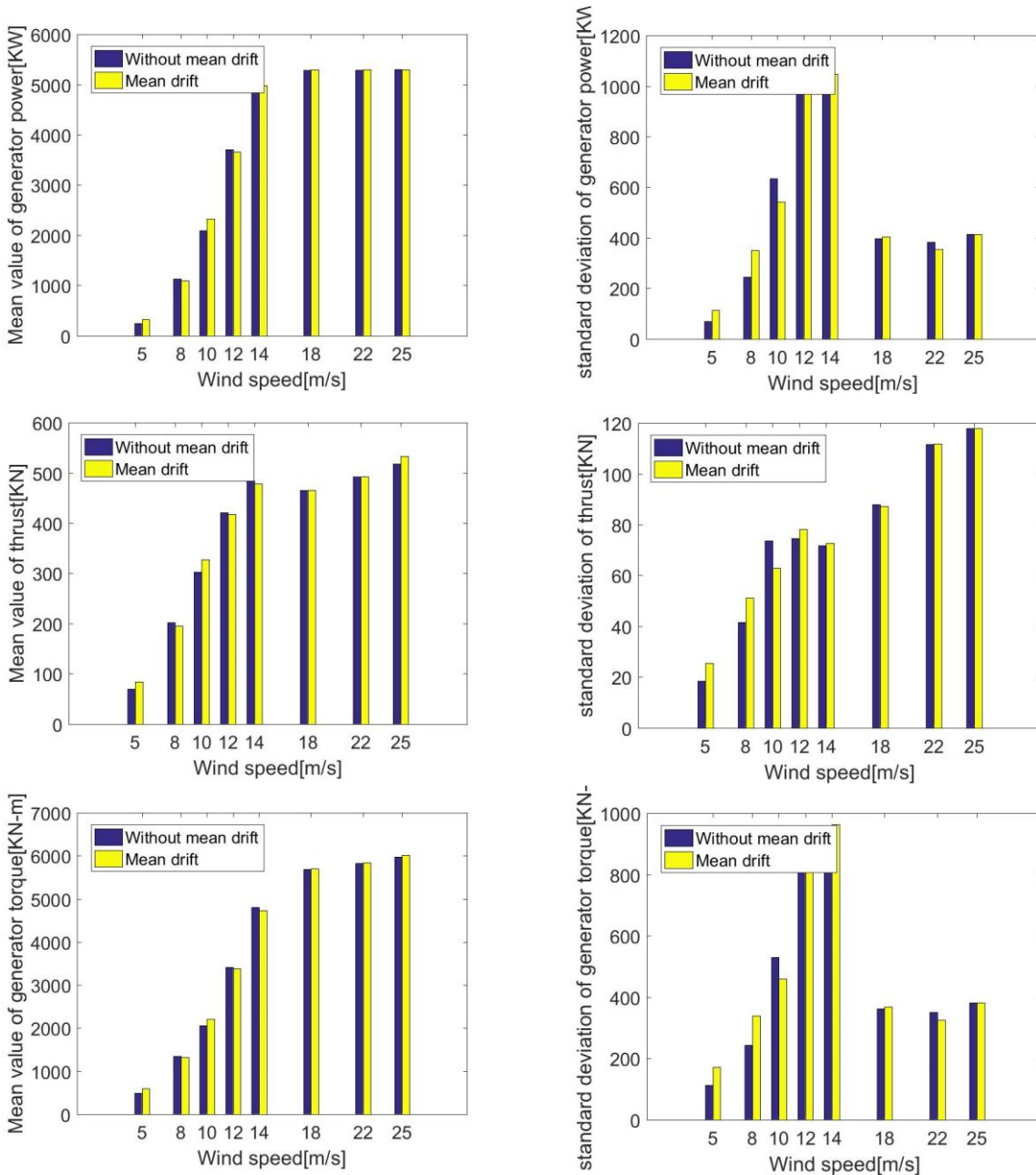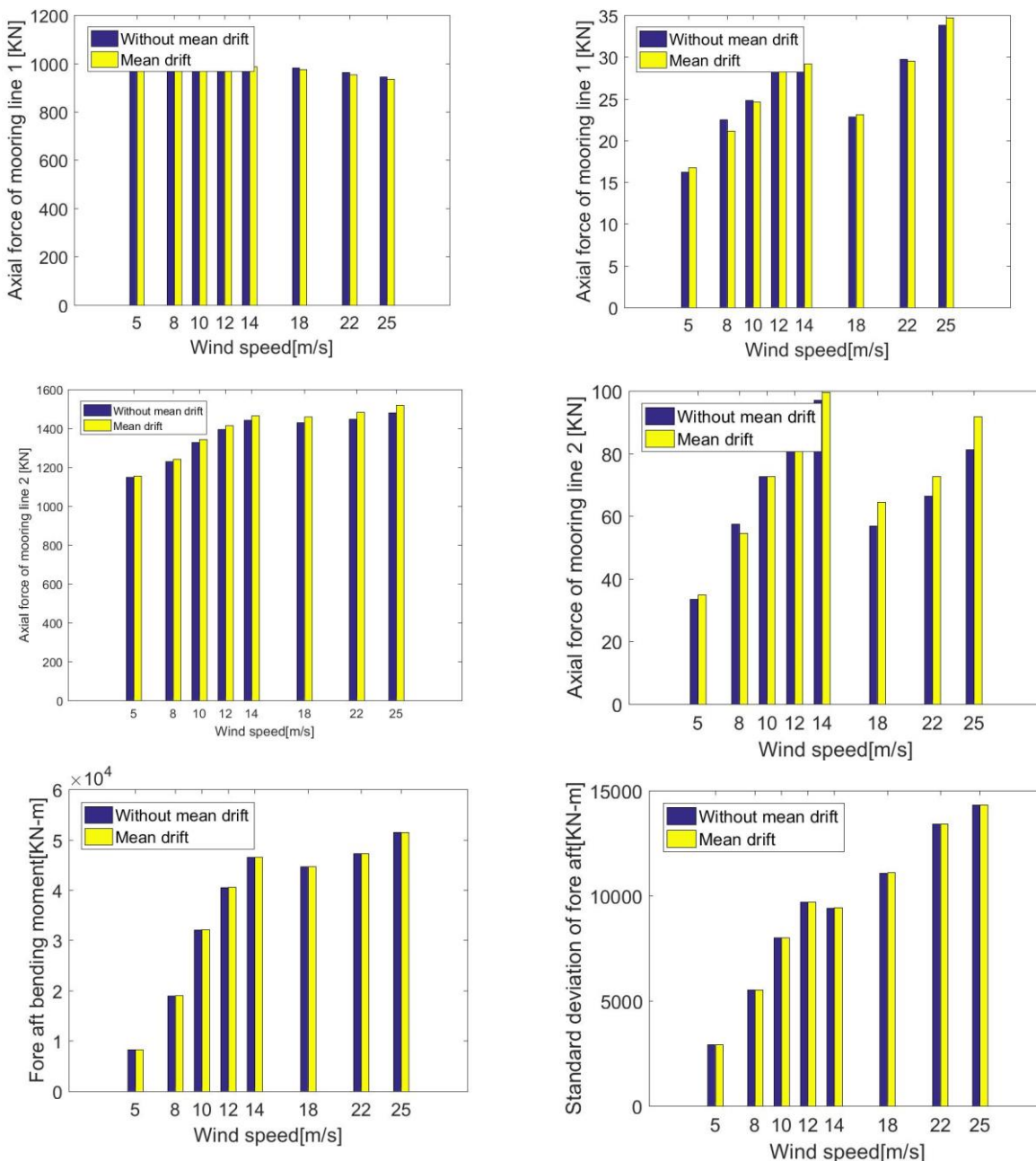
Figure 3.28: Performance of wind turbine (mean drift)

The thrust and torque also follows the same pattern and characteristic response is similar. But there is a discrepancy in the standard deviation due to the variation for mean drift force. But overall the performance is similar.

3.14.3   Tower base bending and mooring line force

The figure shown below compares the result for mean value and standard deviation of tower base bending moment and mooring line tension.
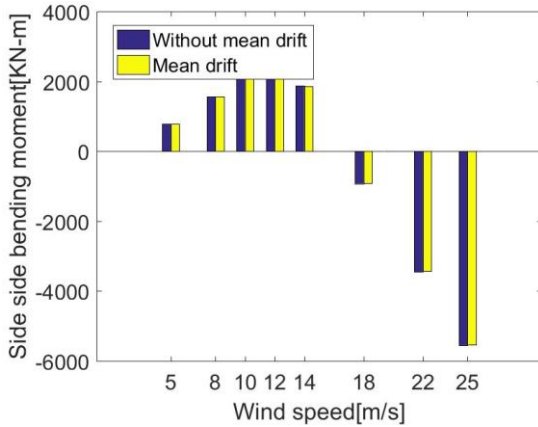
Figure 3.29: Mean value of mooring force on line 1, 2 and fore-aft, side-side bending moment acting on tower base (from up-down)(mean drift)
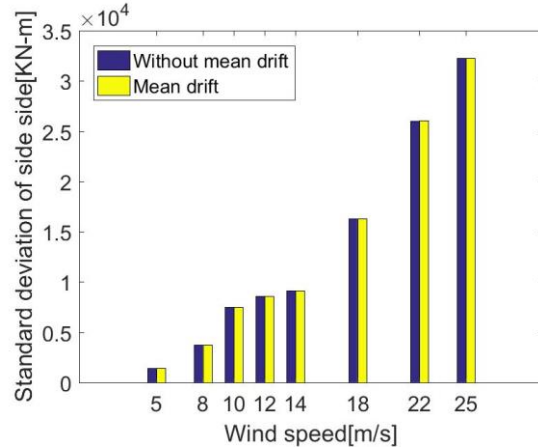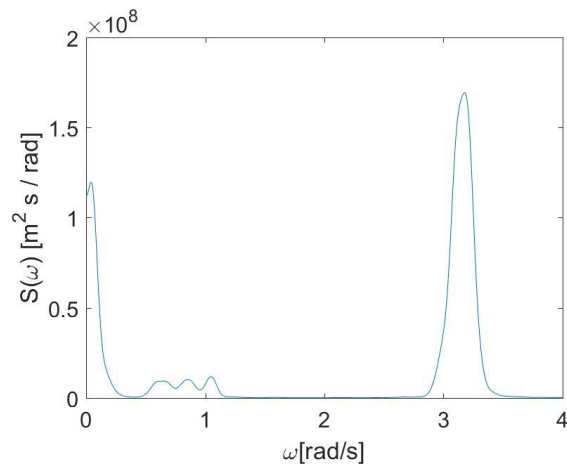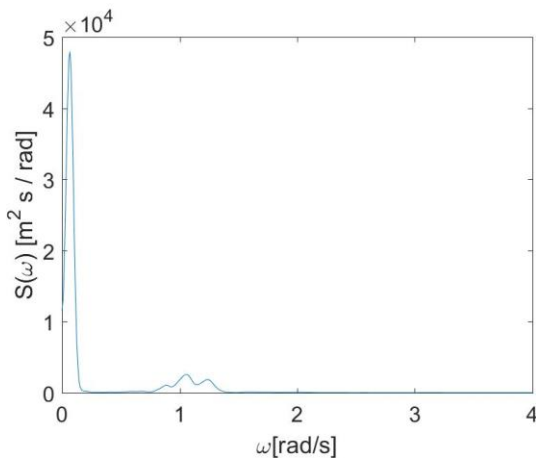

Figure 3.30: Standard deviation of mooring force on line 1, 2 and fore-aft, side-side bending moment acting on tower base (from up-down)(mean drift)

The mooring line tension for the second one is larger than the other mooring line as it was deployed along the direction of wind and wave. The distribution in the first and the third mooring line is almost same due to the symmetry of the platform. Also for the second mooring line the force is increased 20-60 KN due to the wave wind misalignment. The standard deviation is affected than the mean value because the mean value of mooring line forces are primarily determined by the wind loads. But the standard deviation is affected by the frequency component interaction.

The mean and standard deviation of tower base bending moment for the platform for both cases are similar without showing any abrupt changes. The contribution of different cases can be found from the spectrum analysis. The main contributions came from the wind. As for the waves, they increases their interaction as the load cases increases. The figure is shown below:

Figure 3.31: Power spectra for mooring line 2 (LC 2.3, LC 2.5 and LC 2.7)
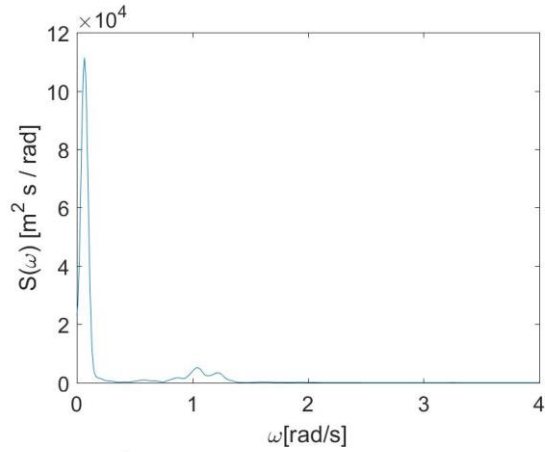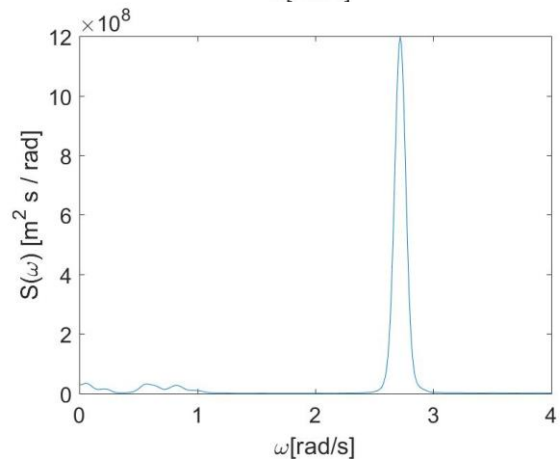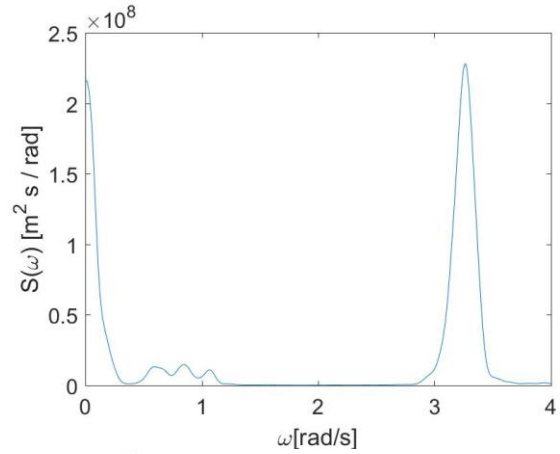
Figure 3.32: Power spectra for tower base bending moment (LC 2.3, LC 2.5 and LC 2.7)

Waves loads effect is seen for mooring line from 0.3-1.5 rad/s and for bending moment the main contribution of waves was in between 0.3-1.2 rad/s. The main response came from the wind loads as seen from each figure which is indicated by the peak resonance near 2.8 rad/s.

Chapter 4

Conclusions and recommendation for future works

4.1   Conclusions

In this study, a FVAWT model was developed based on AC cylinder code originally developed by Madsen and code was developed by Cheng. The code was then coupled with SIMO-RIFLEX, a fully coupled simulation tool used for the time domain simulation for floating VAWT. Then the new model is compared with old OC4 semi-submersible. Using fully coupled simulation tool the performance of the system is carried out. In this thesis, we carried out the motion analysis, performance analysis of the wind turbine, mooring line force and bending moment on the tower base both for steady wind and the turbulent wind and irregular waves. This chapter will deal with the main conclusions and recommendation for future work:

- We developed this new OC4 semi-submersible based on the old OC4 semi-submersible. So, we optimize the parameter and carried out detail calculation whether the platform satisfied the stability criteria. To check the natural frequency and damping ratio we carried out the decay test in SIMO-RIFLEX-AC without calculating any contribution from wind. The result is quite satisfactory. The natural frequency for different motion is outside the range of the first order excitation force. As we mentioned, in this study we reduce the weight of the platform significantly so the stiffness and added mass of the platform decreases which in turn effect the natural frequency of the platform. This was evident from the comparison of both platform. The new model that was developed in this thesis, has reduced natural frequency than the older one.

- Then we carry our analysis for steady wind test. For steady wind test, we use AC method to calculate the aerodynamic loads on the wind turbine. We used a series steady wind test and check the performance. To improve the result, we used BL dynamic stall model. But we neglect the tower shadow, tip loss in our study. This might affect the result a little bit. We check motion of the platform, turbine performance, mooring line tension and bending moment at the tower base. This time we compare three different model and check the output of the result. The result for old OC4 and new OC4 is similar the result for landbased wind turbine is varying in result. The standard deviation of power, torque and thrust varies

greatly. This is one of the disadvantages of wind turbine which trigger the fatigue of the turbine component. But the fatigue of different component can be reduced by applying composite materials. Also, by using improved control strategy we can limit the range of torque and generator power output.

- For turbulent wind and irregular waves there are eight different loading conditions for wind speed and five different turbulent seeds for each loading conditions. We only study on the effect of seed 1 and seed 5. For turbulent wind, we used TurbSim software. The loading effect for wind and wave increases the response of the system. If we look at turbine performance, we can easily verify this. As the loading condition changes the standard deviation is also increased. The standard deviation on mooring line force increase approximately twice than the steady wind condition. The fore-aft bending moment is larger in the tower base. So, we need to employ different strategy to reduce the fore aft bending moment. Otherwise the cyclic loading on the tower base reduce the fatigue life of the wind turbine.

- Finally, we are interested on the topic of second order effect on the system. There are three different types of wave component interaction. They are sum frequency effect, difference frequency effect and mean drift force. Here we only employ the mean drift effect.

4.2   Recommendation for future work

- Here we only consider the normal operating conditions. The simulation in the parked and fault conditions are also of interest.
- The main disadvantages of VAWTs is the less efficiency and severe fatigue problem. To make it sustainable in the long run one need to solve the problem. So, one interesting analysis field is to improve the fatigue conditions of the VAWTs.
- Here we consider three different VAWT models. All of them are straight bladed VAWTs. There are different interesting blade configuration for VAWTs. One can carry out the study for other rotor type such as helical bladed rotor, Savonius rotor etc.
- A Pi generator controller is employed in this study. An improved control strategy could be designed to maintain the constant power by reducing the rotational speed of the rotor at high wind speed.
- Drift force is the only second order effect that we study here. But one can also extend the study and investigate the slowly varying drift force and sum frequency effect on the total system.
- Here we only look at the OC4 floater for VAWT. But a comparison on FHAWT and FVAWT will further reveals the advantages and disadvantages of the two model. Also, OC4 FVAWT concept need to compare with other floater such as TLP, Spar. Moreover, the investigation might expand for H-type, V-type and helical-bladed rotor.

References

[1] E. Hau, Wind turbines: fundamentals, technologies, application, economics, Springer Science & Business Media, 2013.

[2] T. J. N. Burton, D. Sharpe and E. Bossanyi, Wind Energy Handbook, John Wiley & Sons., 2011.

[3] https://en.wikipedia.org/wiki/Wind_power.

[4] "Global wind statistics 2016," Global wind energy council, 2017.

[5] Z. Cheng, "Integrated Dynamic Analysis of Floating Vertical Axis Wind Turbines," 2016.

[6] Paulsen, Uwe. S. et al. "Outcomes of the DeepWind conceptual design," Energy Precedia vol. 80, pp. 329-341, 2015.

[7] "http://www.inflow-fp7.eu/floating-vertical-axis-wind-turbine/".

[8] M. Borg, M. Collu and F. P. Brennan, "Offshore floating vertical axis wind turbines: advantages, disadvantages, and dynamics modelling state of the art," *The International Conference on Marine & Offshore Renewable Energy* , 2012.

[9] P. Jamieson, "Innovation in Wind Turbine design," *John Wiley & Sons,* 2011.

[10] X. Jin, G. Zhao, K. Gao and W. Ju, "Darrieus vertical axis wind turbine: Basic research methods," *Renewable and Sustainable Energy Reviews* , vol. 42, pp. 212-225, 2015.

[11] H. C. Larsen, "Summary of a vortex theory for the cyclogiro," *Proceedings of the 2nd US National conference on Wind Engineering Research.(1975-8), Colorad State University,* vol. 8, 1975.

[12] J. B. Fanucci, Walters and R. E., "Innovative wind machines: The theoretical performances of a vertical axis wind turbine," *Proc. Of the VAWT Technology Workshop, Sandia Lab.,* 1976.

[13] Holme, "Contribution to the aerodynamic theory of the vertical axis," *International symposium on wind energy systems,* Vols. C4,7-9, pp. 55-71.

[14] R. E. Wilson, "Wind-turbine aerodynamics," *Journal of Wind Engineering and Industrial Aerodynamics,* Vols. 5.3-4, pp. 357-372, 1980.

[15] J. H. Strickland, B. T. Webster and T. Nguyen, "A vortex mdoel of the darrieus turbine: an analytical and experimental study," *Sandia National,* 1981.

[16] J. L. Cardona, "Flow curvature and dynamic stall simulated with an aerodynamic free-vortex model for VAWT," *Wind Engineering,* pp. 135-143, 1984.

[17] H. A. Madsen, The Actuator Cylinder: A flow model for Vertical Axis Wind Turbine, Institute of Industrial Constructions and Energy Technology, Aalborg University Centre, 1982.

[18] I. Paraschiviou, Wind turbine design: emphasis on the darrieus concept, 1 ed., Montreal: Polytechnic International Press, 2001.

[19] J. H. Strickland, B. T. Webster and T. Nguyen, "Vortex model of the darrieus turbine: an analytical and experimental study," *American Society of Mechanical Engineers,* 1979.

[20] K. Dixon, "The near wake structure of a vertical axiswind turbine (Master's thesis)," TU Delft, Netherlands, 2009.

[21] Z. Cheng, H. A. Madsen, Z. Gao and T. Moan, "A fully coupled method for numerical modeling and dynamic analysis of floating vertical axis wind turbines," *Renewable Energy,* vol. 107, pp. 604-619, 2017.

[22] L. TJ and H. AM., How 2 HAWC2, the user's manual, Risø National Laboratory, Technical University of Denmark, 2013.

[23] D. N. Veritas, DNV-OS-J103: Design of Floating Wind Turbine Structures., 2013.

[24] Z. Cheng, H. A. Madsen, Z. Gao and T. Moan, "Aerodynamic modeling of floating vertical axis wind turbines using the actuator cylinder flow method," *ScienceDirect,* vol. 94, pp. 531-543, 2016.

[25] A. Robertson, J. Jonkman, M. Masciola and e. al, "Definition of the semisubmersible floating system for phase II of OC4. No. NREL/TP-5000-60601," National Renewable Energy Laboratory (NREL), Golden, CO.,, 2014.

[26] H. Aagard Madsen, T. J. Larsen, U. Schimdt Paulsen and L. Vita, "Implementation of the Actuator Cylinder Flow Model in the HAWC2 code for Aeroelastic Simulations on Vertical Axis Wind Turbines," *DTU orbit,* p. 12, 2013.

[27] C. M. Larsen, Marine Dynamics, Trondheim: Department of Marine Technology, NTNU, 2015.

[28] M. Greco, Lecture notes on Sea loads, 2012.

[29] P. J. Moriarty and A. C. Hansen, "AeroDyn theory manual," National Renewable Energy Lab., Golden, CO (US), 2005.

[30] O. Faltinsen, Sea Loads on Ships and Offshore Structures, vol. 1, Cambridge University Press, UK, 1993.

[31] B. J. Jonkman, "TurbSim user's guide: Version 1.50," 2009.

[32] L. Vita, T. Friis Pedersen and H. Aagaard Madsen, "Offshore Vertical Axis Wind Turbine with Floating and Rotating Foundation," Technical University of Denmark, 2011.

[33] Z. Cheng, H. A. Madsen, Z. Gao and T. Moan, "Effect of number of blades on the dynamics of floating straight-bladed vertical axis wind turbines," *Renewable Energy,* vol. 101, pp. 1285-1298, 2017.

[34] J. Wayne, Rotorcraft Aeromechanics, vol. 36, Cambridge university press, 2013.

[35] M. Leimeister, Rational Upscaling and Modelling of a Semi Submersible Floating Offshore Wind Turbine, Trondheim: NTNU, TU Delft, 2016.